4. Electronic Structure, Magnetism and Pairing in Fe-Based Superconductors

David J. Singh

Materials Science and Technology Division, Oak Ridge National Laboratory, Oak Ridge, TN 37831-6114, USA

The physical properties of the layered iron superconductors are discussed starting from first principles calculations. The electronic structure is described as that of metallic Fe^{2+} square lattice sheets with substantial direct Fe-Fe hopping and interactions with the neighboring anionic pnictogens or chalcogens. The materials have a semi-metallic band structure, and in particular the Fermi surface consists of small cylindrical electron sections centered at the zone corner, and compensating hole sections at the zone boundary. The density of states at the Fermi energy is high placing the materials near itinerant magnetism in general, and furthermore the Fermi surface is well nested, leading to a tendency towards a spin density wave. Comparison of experimental and density functional results imply the presence of exceptionally strong spin fluctuations in these materials. We discuss pairing and superconductivity within this context.

This work was supported by the Department of Energy, Division of Materials Sciences and Engineering.

Electronic Structure Magnetism and Pairing in Fe-Based Superconductors

David J. Singh
Oak Ridge National Laboratory

Co-workers (Theory):

M.H. Du (ORNL)
A. Subedi (ORNL)
L. Zhang (ORNL)
H. Takenaka (ORNL)
I.I. Mazin (NRL)
M.D. Johannes (NRL)

Collaborations/Discussion:

B.C. Sales, D. Mandrus,
A.S. Sefat, M. McGuire (ORNL)
Z.X. Shen, D. Lu (Stanford)
N. Mannella, T. Egami (U.T.)

Supported by DOE, Division of Materials Sciences and Engineering.

January 25, 2009

Discovery of Superconductivity in Fe-As Compounds

Kamihara *et al.*, JACS, 2006

LaFePO, $T_c \sim 4$K

Kamihara, Watanabe and Hosono, JACS, Feb. 2008

$LaFeAsO_{1-x}F_x$ T_c=26K

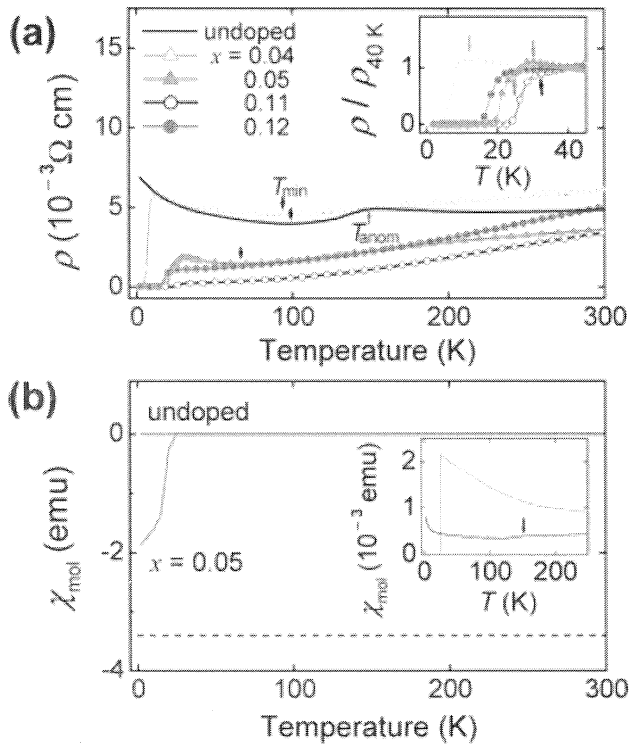

Fe-based Superconducting Families

LaFeAsO	$BaFe_2As_2$	LiFeAs	FeSe
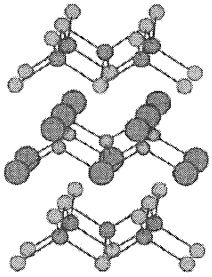	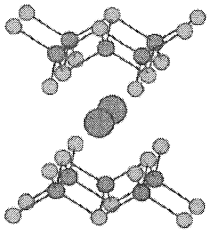	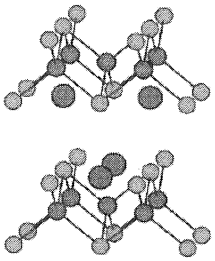	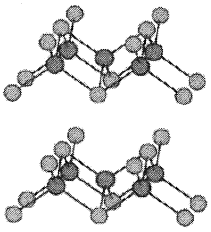
ZrSiCuAs	$ThCr_2Si_2$	LiMnAs	PbO
P4/nmm	*I4/mmm*	*P4/nmm*	*P4/nmm*
~55K	~40K	~20K	~25K

Superconductivity is robust. Occurs across a broad range of compositions, including replacement of As, and doping on the Fe site.

FeSe - The "Simplest" Fe-Superconductor

- Simple tetragonal structure, four atoms per unit cell (Hagg and Kindstrom, Z. Phys. Chem. (1933).
  - Actual material is $Fe_{1+x}Se$, with extra Fe in holes of Se lattice.
  - LiFeAs is similar, but extra sites are filled with Li.

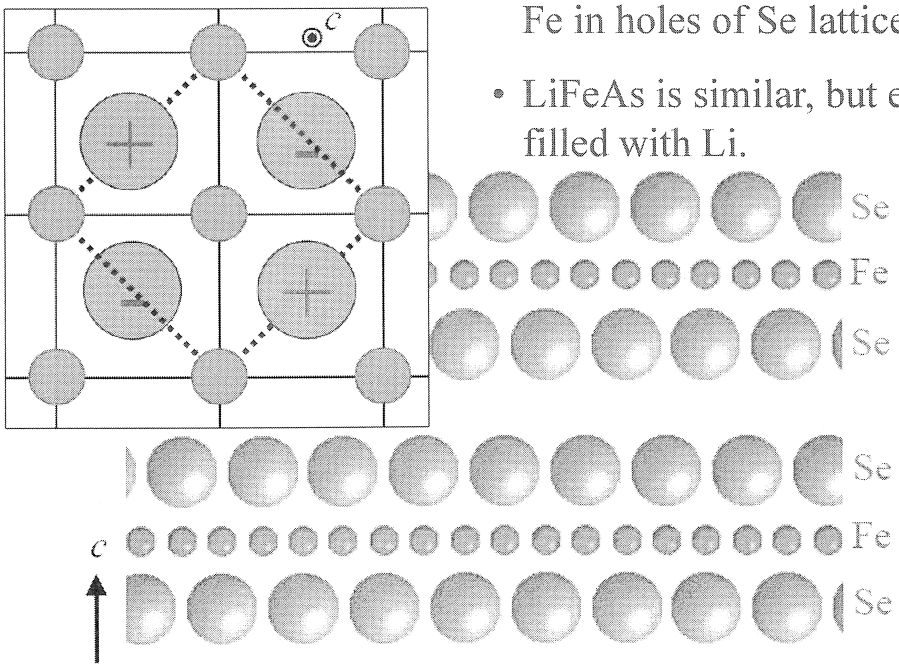

$d_{Fe\text{-}Fe}$= 2.66 Å

LDA Electronic Structure of FeSe

- A rather ionic material – Fe^{2+} and Se^{2-} with some hybridization, as in an oxide ➔ metallic sheets of Fe^{2+} modified by interaction of anions.
- Pauling electronegativities: Fe = 1.83; Se = 2.55; As = 2.18.

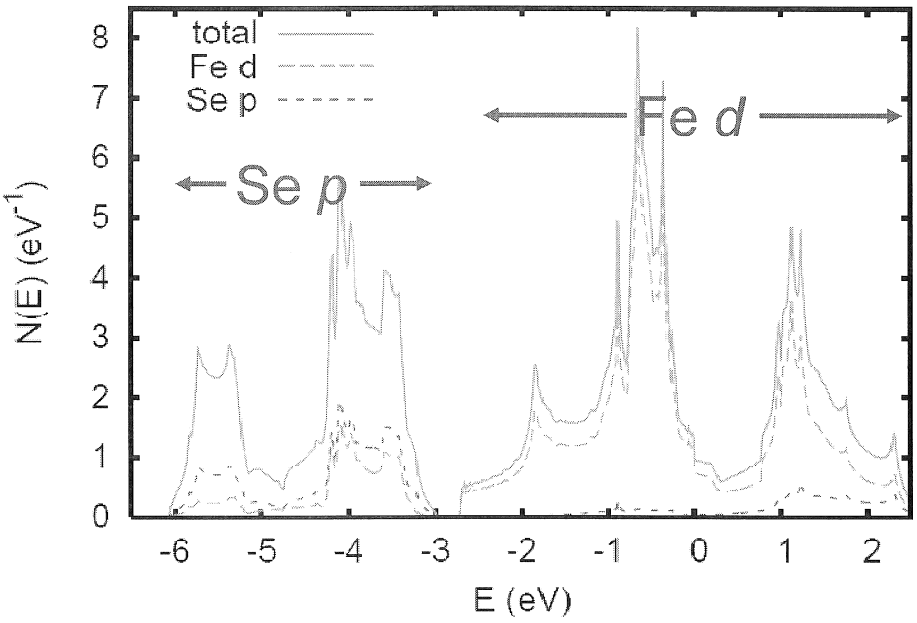

Fe^{2+} ➔ d^6

$N(E_F)$ is at bottom of pseudogap.

Arsenide Electronic Structure: LaFeAsO

- LaFeAsO: Rather ionic electronic structure: O^{2-}, As^{3-}, La^{3+}
- Bands near E_F are derived from Fe with little As admixture

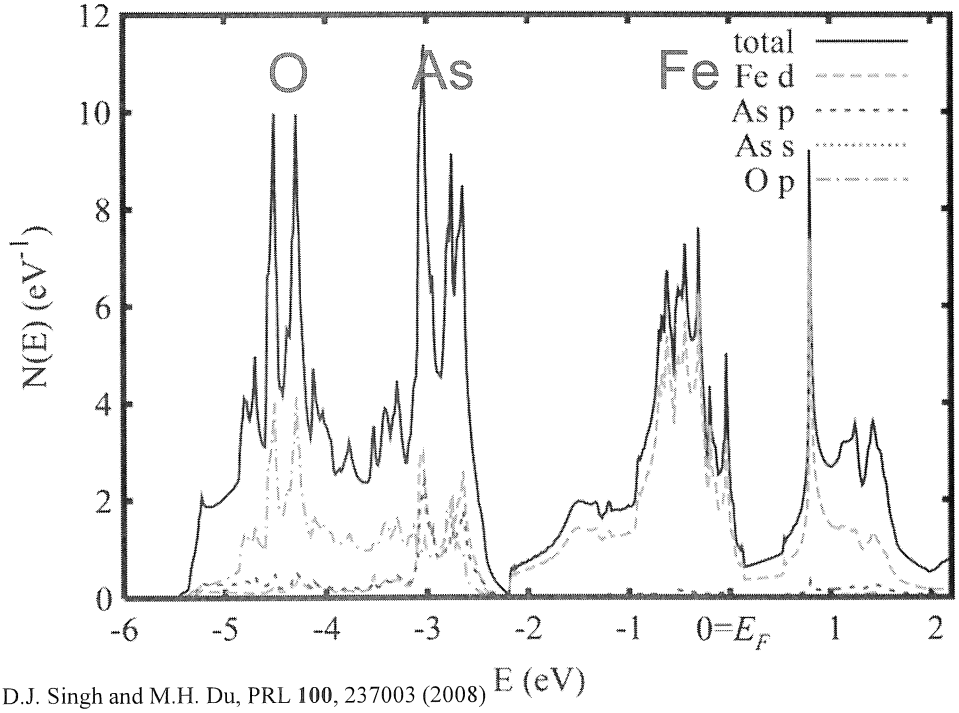

Metallic sheets of Fe^{2+}

E_F is at the bottom edge of a pseudogap

High $N(E_F)$ ➔ near magnetism

D.J. Singh and M.H. Du, PRL **100**, 237003 (2008)

Formation of Band Structure

- Bands from -2 eV to +2 eV are derived from Fe^{2+} *d*-states.
- Fe^{2+} has 6 *d*-electrons.

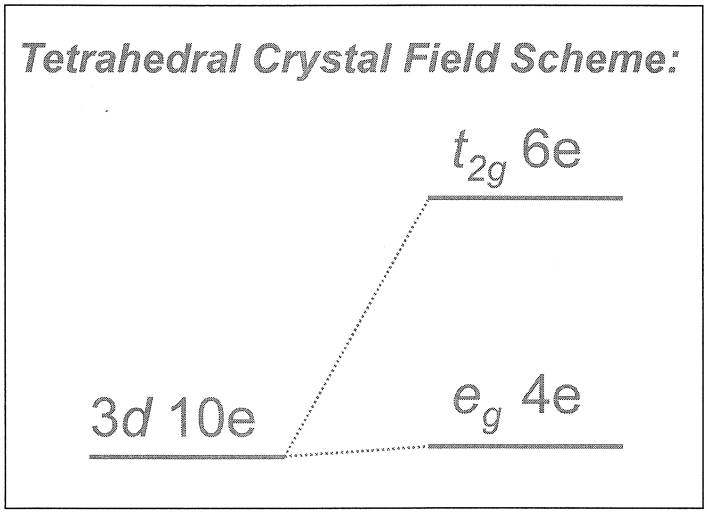

Does not correspond to the calculated electronic structure.

Key is the short Fe-Fe bond length → direct Fe-Fe interactions.

Coulomb Correlations

- LDA and correlated approaches give rather different predictions.
- So far experiment aligns better with LDA.
- Not Coulomb correlated in the sense of cuprates.

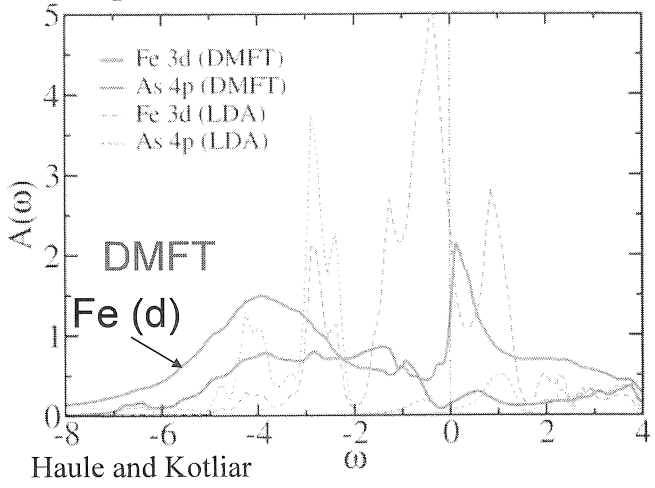

Haule and Kotliar

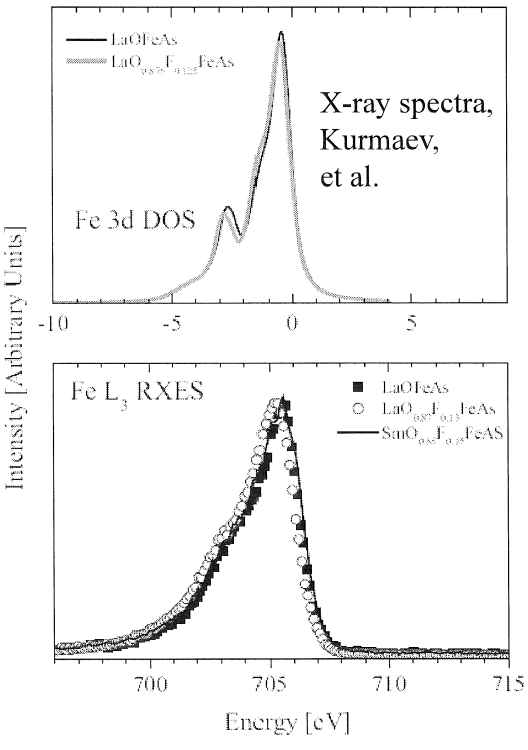

Fermi Surface LaFeAsO – Non-Spin-Polarized

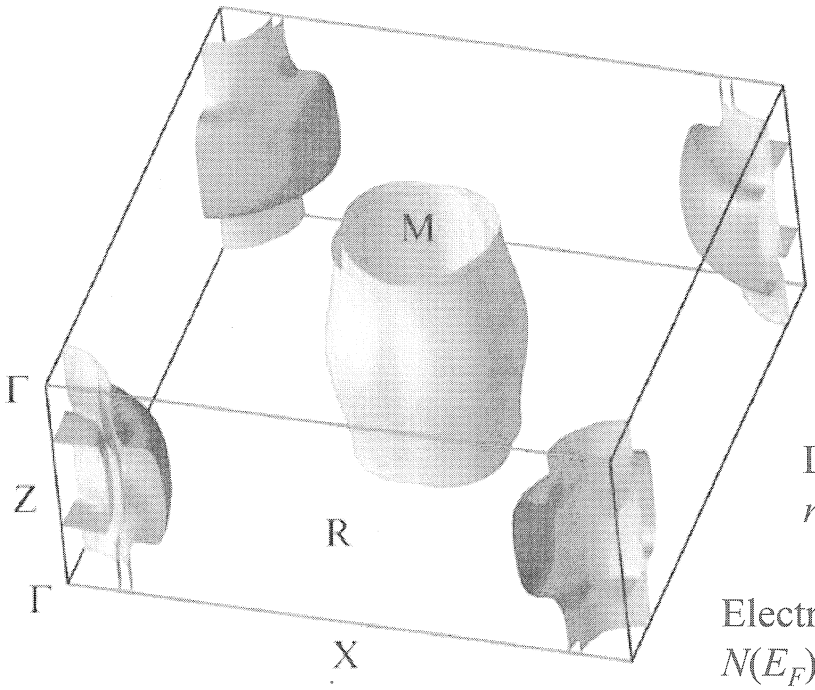

Two cylindrical electron sections at zone corner.

Two cylindrical hole sections at zone center.

3D hole section at zone center.

Low carrier density: $n_e=n_h=0.13$ / Fe

Electrons provide 20% of $N(E_F)$ but 65% of $N\langle v_x^2\rangle$

Band anisotropy: $\langle v_x^2\rangle / \langle v_z^2\rangle \sim 15$ ➔
a modest value that is favorable for applications.

Normal Metallic State

- Low carrier density semi-metal (dis-connected small Fermi surfaces).
- Less anisotropic than cuprates, even $YBa_2Cu_3O_7$.
- High $N(E_F)$.
  - Near itinerant magnetism in general.
  - Expect short coherence length relative to T_c.
  - Expect high superfluid density.
- Electron-Phonon interaction is weak ($\lambda\sim0.2$, $T_c=0$)

Superconductivity in Metal Doped Materials

- Superconductivity requires destruction of SDW by doping.
- Remarkably, doping with Co or Ni works (*c.f.* cuprates).

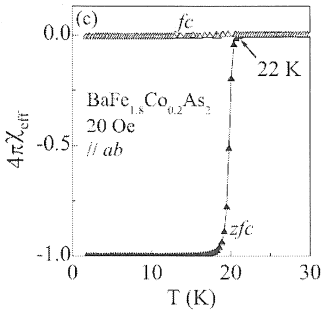

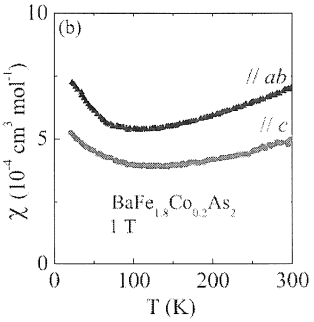

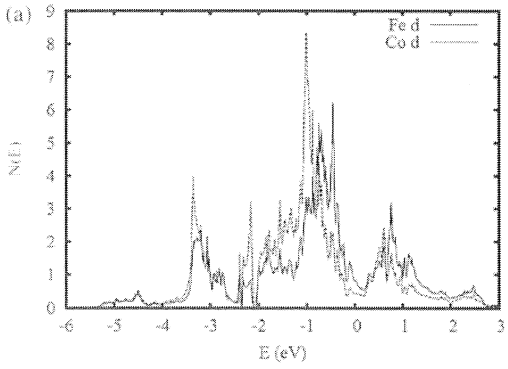

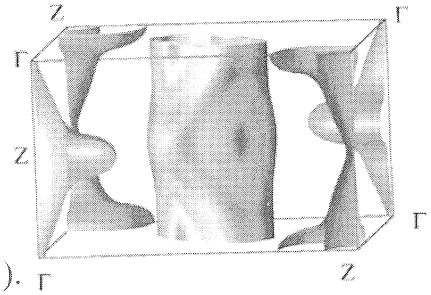

A.S. Sefat, et al., PRL (2008).

Calculations show that alloy behaves very much in a rigid band sense.

Fe-Co-Ni behave very similarly apart from electron count.

Mn and Cr show strong spin dependent hybridization (different).

Chemical Details Matter

- The detailed Fermi surface structure especially for the hole bands depends on the material ➔ can the different properties be understood in terms of these?

LaFeAsO:

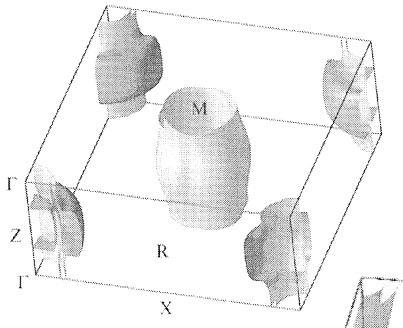

LiFeAs:

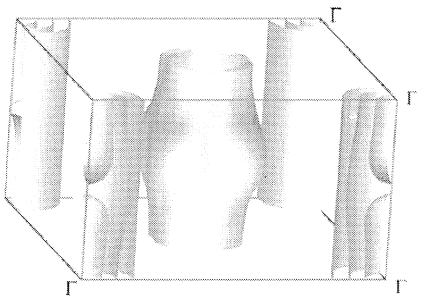

FeSe:

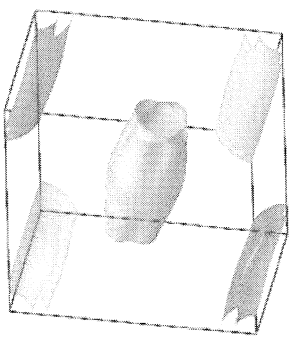

$BaFe_2As_2$

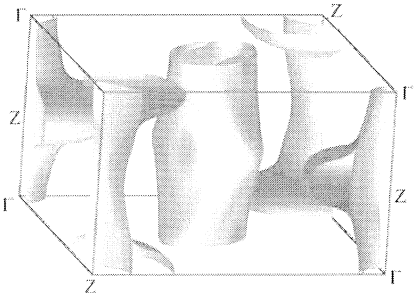

Experimental Situation

- ARPES and dHvA (phosphide) support general band and Fermi surface picture, but with mass renormalization of ~2.
- No large deviation is found on the energy scale of 1 – 5 eV. In particular no feature identifiable as a lower or upper Hubbard band is seen. Contradicts strong coupling picture as in DMFT calculations.

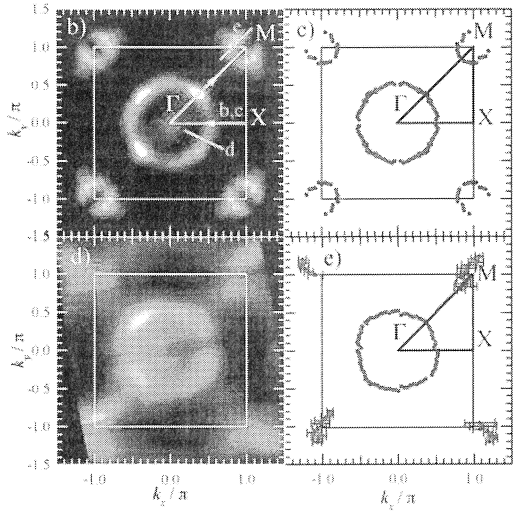

Electron doped NdFeAs(O,F)

Some problems (reconstruction?), but general topology is reproduced.

C. Liu et al., arXiv:0806.2147

Multiband Superconductivity

$LaFeAsO_{0.89}F_{0.11}$ (T_c ~ 26K):

F. Hunte et al., Nature **453**, 903 (2008)

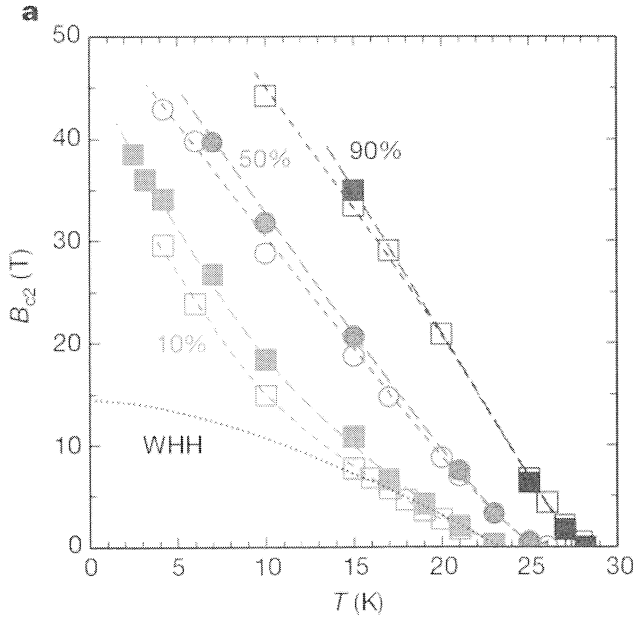

Shape shows two band superconductivity

Upper critical fields (from lower field extrapolation) of higher T_c compounds exceed 100T.

LaFeAs(O,F) Lindhard Function

- Neglecting Matrix Elements:

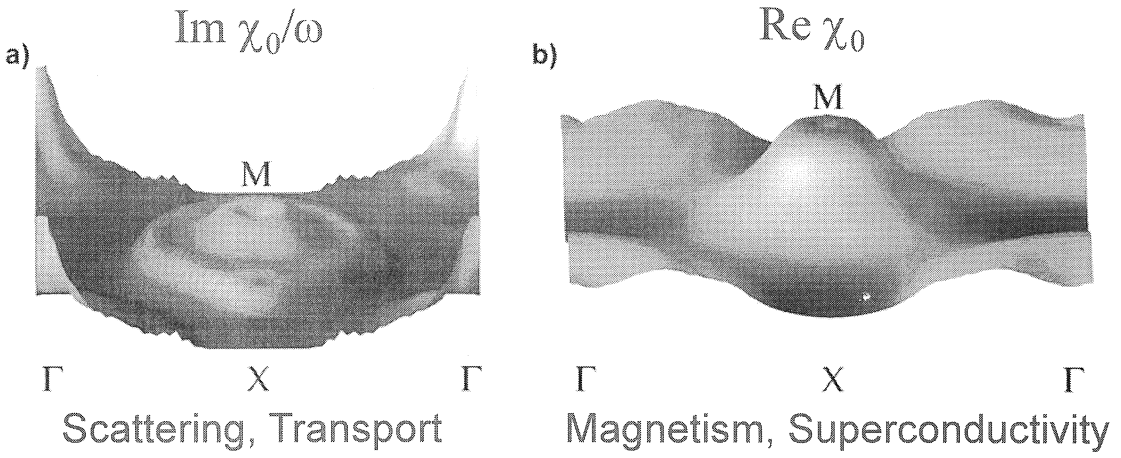

Note the pronounced peak at the zone corner.

I.I. Mazin, D.J. Singh, M.D. Johannes and M.H. Du, PRL **101**, 057003 (2008)

Spin Fluctuations and Superconductivity

One way to proceed (weak coupling):

- Calculate matrix elements $V_{k,k'}$, for a set of **k**,**k**' on the FS.
- Set-up gap equation -- diagonalize V.

Berk-Schrieffer-Fay-Appel weak coupling theory, 1966-1980:

Singlet:

$$V(\mathbf{q}) = - \frac{I^2(q)\chi_0(\mathbf{q})}{1 - I^2(\mathbf{q})\chi_0^2(\mathbf{q})}$$

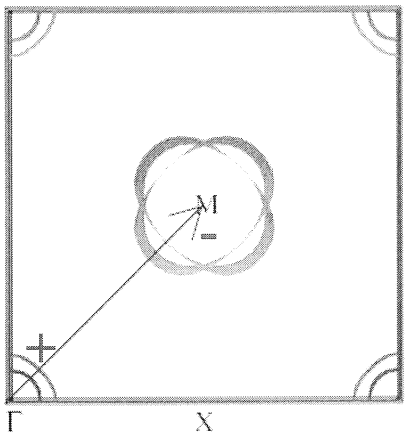

Electron doped LaFeAsO

In a singlet channel there is a minus sign for spin fluctuations (repulsive), which then favors opposite order parameters on the electron and hole sheets ➔ s +/- state.

Note prior work, Aronov & Sonin (1972); Kuroki and Arita (2001)

Does not have an obvious strongly q-dependent interaction for nodes in a FS.

I.I. Mazin, D.J. Singh, M.D. Johannes and M.H. Du, PRL **101**, 057003 (2008)

S +/- Superconducting Properties

- Two gap.
- SDW and superconductivity are driven by the same interaction and compete for the same electrons.
- Clean limit thermodynamics is exponential.
- Clean gap in tunneling.
- Robust against low *q* scattering (Co, Ni doping?)
- No corner junction shifts (*s*-wave symmetry)
- Coherence factors depend on q. Reduced Hebel-Slichter peak in NMR relaxation rate.
- Resonance peak in neutron scattering.

Small Fermi Surfaces in General

- Does superconductivity arise in general if one has small Fermi surfaces with nesting driven spin fluctuations? – Answer seems to be no.

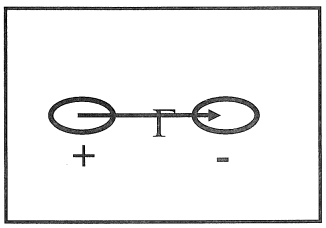

p-wave state (triplet): spin-fluctuation pairing interaction has + sign ➔ Pair breaking for the state shown.

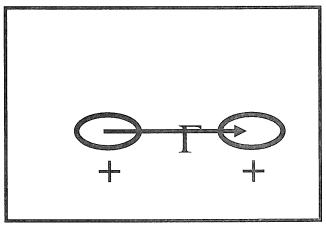

s-wave state (singlet): spin-fluctuation pairing interaction has – sign ➔Pair breaking for the state shown.

e.g. small pockets on Na_xCoO_2 (Johannes et al., 2004).

In such cases, look for chemistry with strong electron phonon and low Stoner parameter, to obtain Kohn anomaly and e-p superconductivity or maybe strange states, e.g. odd frequency.

nature Vol 456|18/25 December 2008|doi:10.1038/nature07625

LETTERS

Unconventional superconductivity in $Ba_{0.6}K_{0.4}Fe_2As_2$ from inelastic neutron scattering

A. D. Christianson[1], E. A. Goremychkin[2,3], R. Osborn[2], S. Rosenkranz[2], M. D. Lumsden[1], C. D. Malliakas[2,4], I. S. Todorov[2], H. Claus[2], D. Y. Chung[2], M. G. Kanatzidis[2,4], R. I. Bewley[3] & T. Guidi[3]

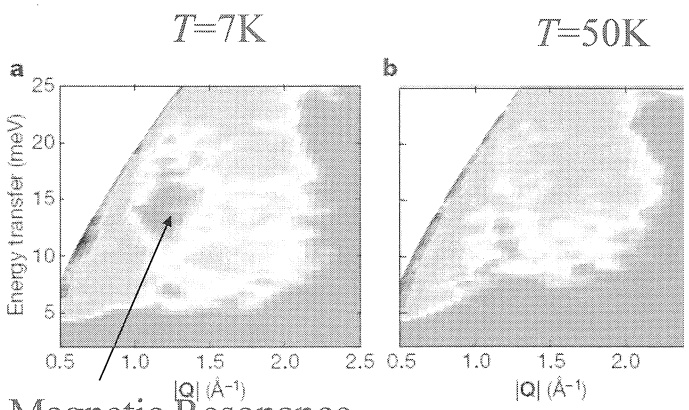

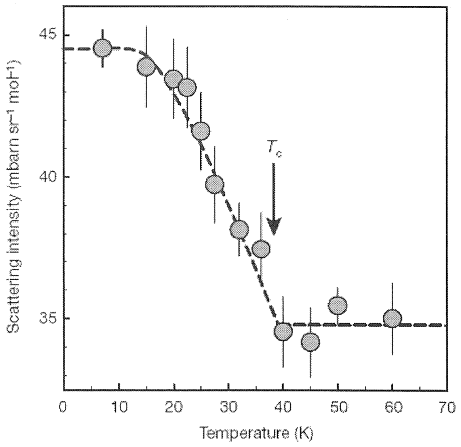

Magnetic Resonance

Sign changing gap with q corresponding to (π,π)

Gap Structure

Fully Gapped: Andreev reflection, ARPES penetration depth (oxy-arsenides), tunneling.

Power Law (e.g. Line Nodes): NMR. Penetration depth on $Ba(Fe,Co)_2As_2$.

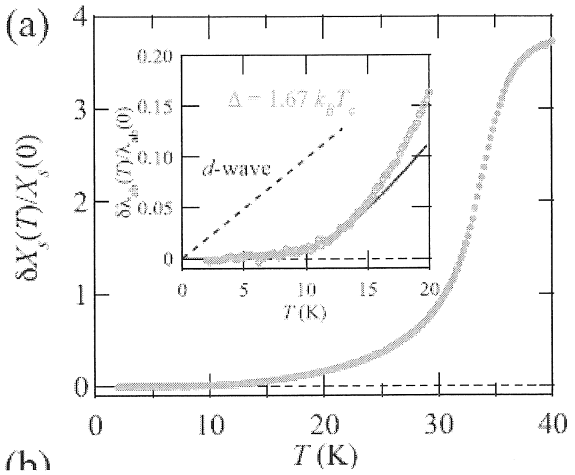

BCS $\dfrac{\delta\lambda_{ab}(T)}{\lambda_{ab}(0)} \approx \sqrt{\dfrac{\pi\Delta}{2k_BT}}\exp\left(-\dfrac{\Delta}{k_BT}\right)$

Microwave penetration depth, $PrFeAsO_{1-x}$
K. Hashimoto, et al., PRL (2009).

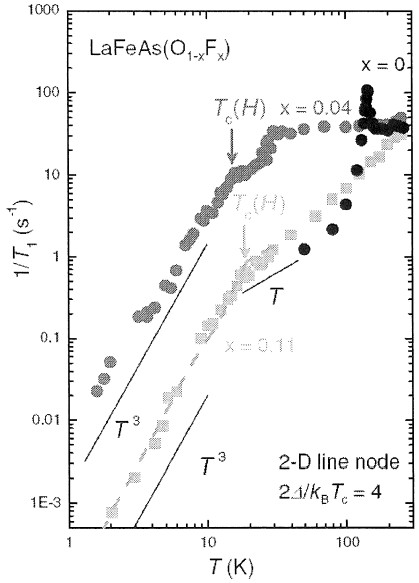

NMR, LaFeAs(O,F)
Y. Nakai, et al., JPSJ (2008).

Neutron Scattering – Magnetism & Structure

LaFeAsO:

Ordered m(Fe) = 0.36 μ_B

(other compounds so far are between 0.3 and 1 μ_B)

C. de la Cruz et al., Nature **453**, 899 (2008)

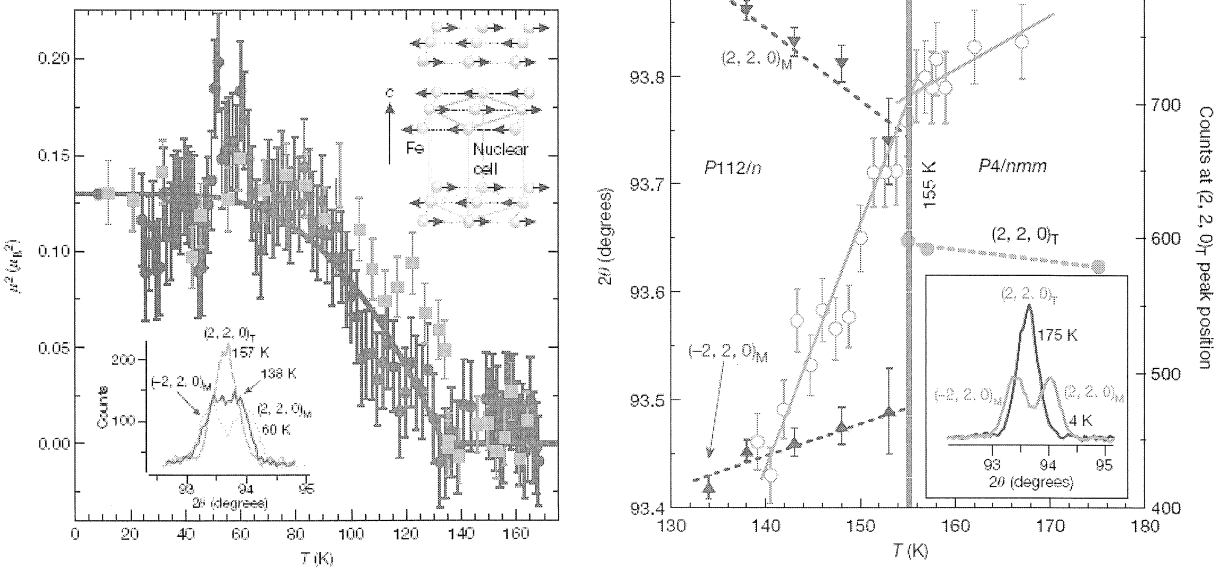

In-plane SDW structure

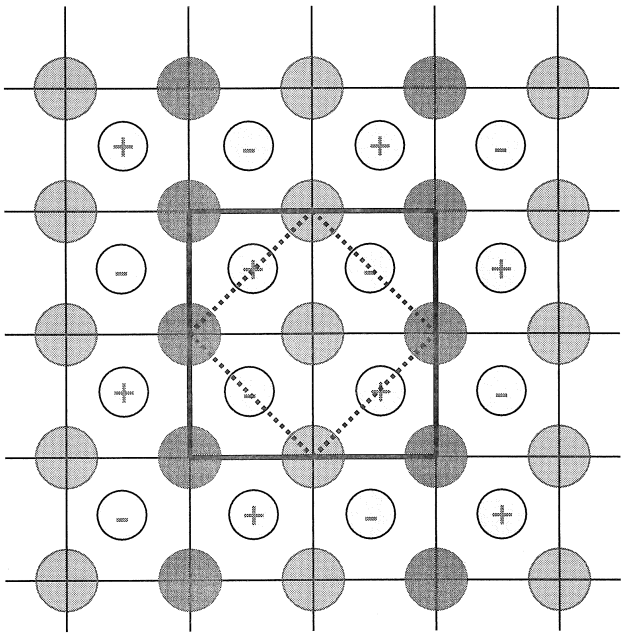

1 D Chains of parallel spin Fe atoms.

Resistivity in LaFeAsO

McGuire *et al.* (cond-mat):

Resistivity:

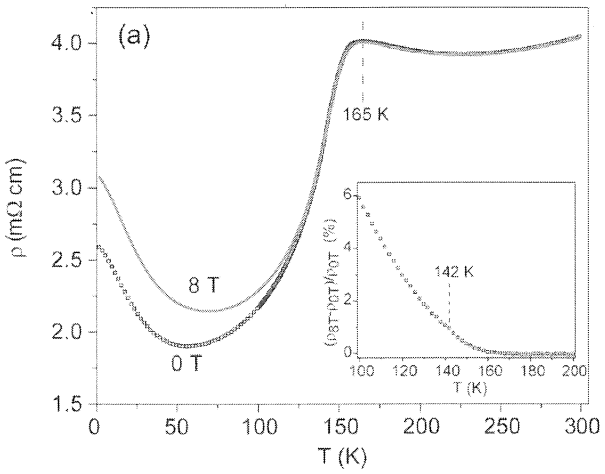

Hall:

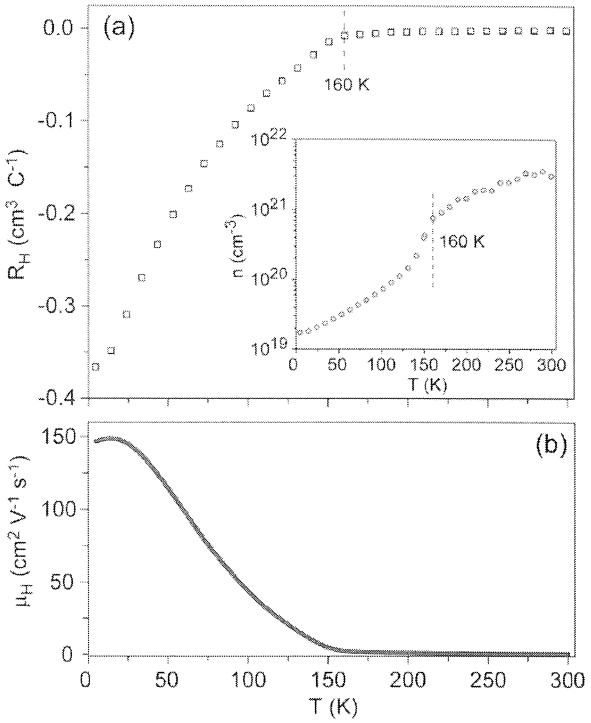

Evidence of strong interplay of magnetic ordering and Fermi surface.

Evidence of spin fluctuations.

Structure and Magnetism

- As height is too low by ~0.1 Å in non-magnetic LSDA calculations.
- SDW is too robust compared to experiment.
- Using GGA and including magnetism one can obtain much better As height. In that case magnetism is extremely robust (m~2μ_B) contrary to experiment.
- Discrepancy in As height persists in the paramagnetic (superconducting) doped phases.
- There is a strong isotope effect both on T_c and on T_{SDW} (Liu *et al.*, cond-mat, 2008).
- We take this as an indication of very strong non-trivial spin-fluctuations.

Quantum Critical Points and the LDA

Density Functional Theory: LDA & GGA are widely used for first principles calculations but have problems:

- Mott-Hubbard: Well known poor treatment of on-site Coulomb correlations.
- Based on uniform electron gas. Give mean field treatment of magnetism: Fluctuations missing.

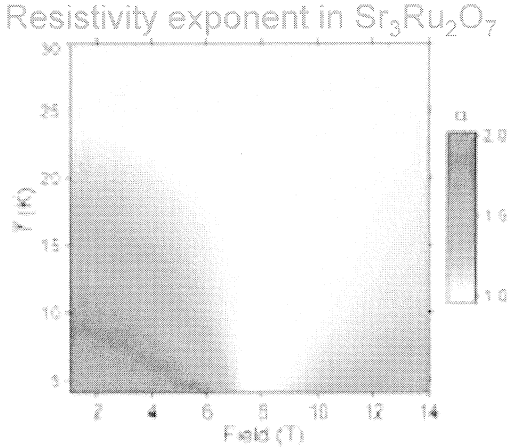

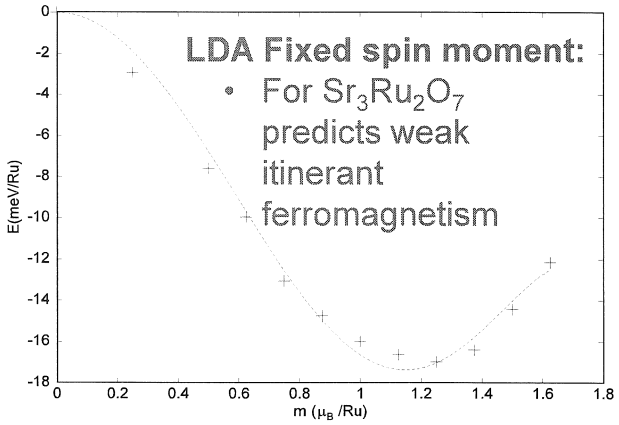

Grigera *et al.*, Science (2001).

LDA overestimate of ferromagnetic tendency is a signature of quantum critical fluctuations – neglected fluctuations suppress magnetism

Strong Spin Fluctuations in Normal State

- Transport data.
- Susceptibility - $\chi(T)$.
- Spectroscopy.
- Scattering.
- Overly magnetic in LDA.
- Precursor structural transition.

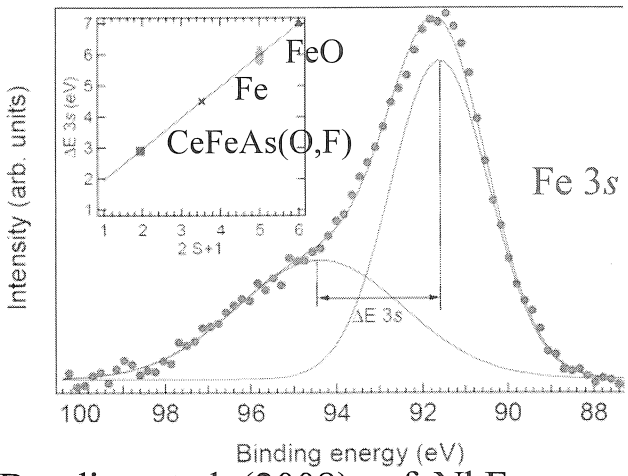

Bondino et al. (2008); c.f. $NbFe_2$

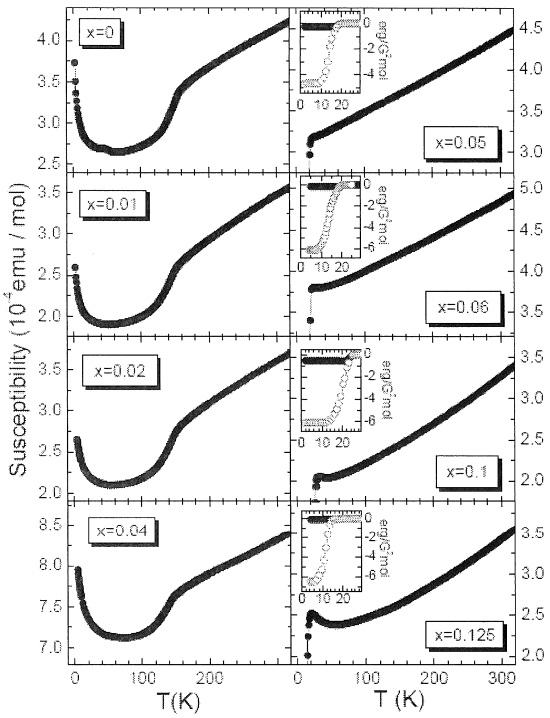

R. Klingeler et al., cond-mat

$LaFeAsO_{1-x}F_x$

Hund's Coupling

- Hund's coupling in 3d ions is strong (Stoner I~0.8 eV)
- Spin-fluctuations are then expected to couple to electronic states in the d-band going up to high energy (i.e. the d-band width) – may be observable in spectroscopy. Drude weight seems reduced in optics.

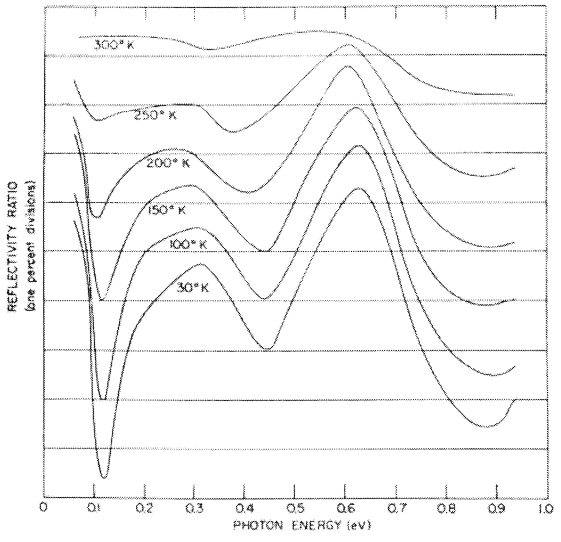

Fig. 3. The temperature dependent reflectivity of chromium normalized to T=400 K.

Cr metal: Machida et al., JPSJ (1984).

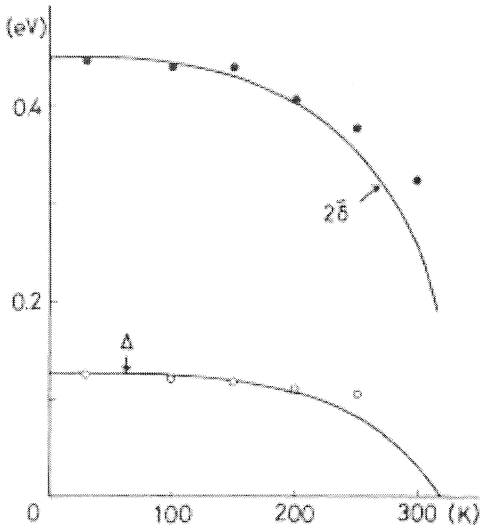

Nesting, Doping and the Lindhard Function

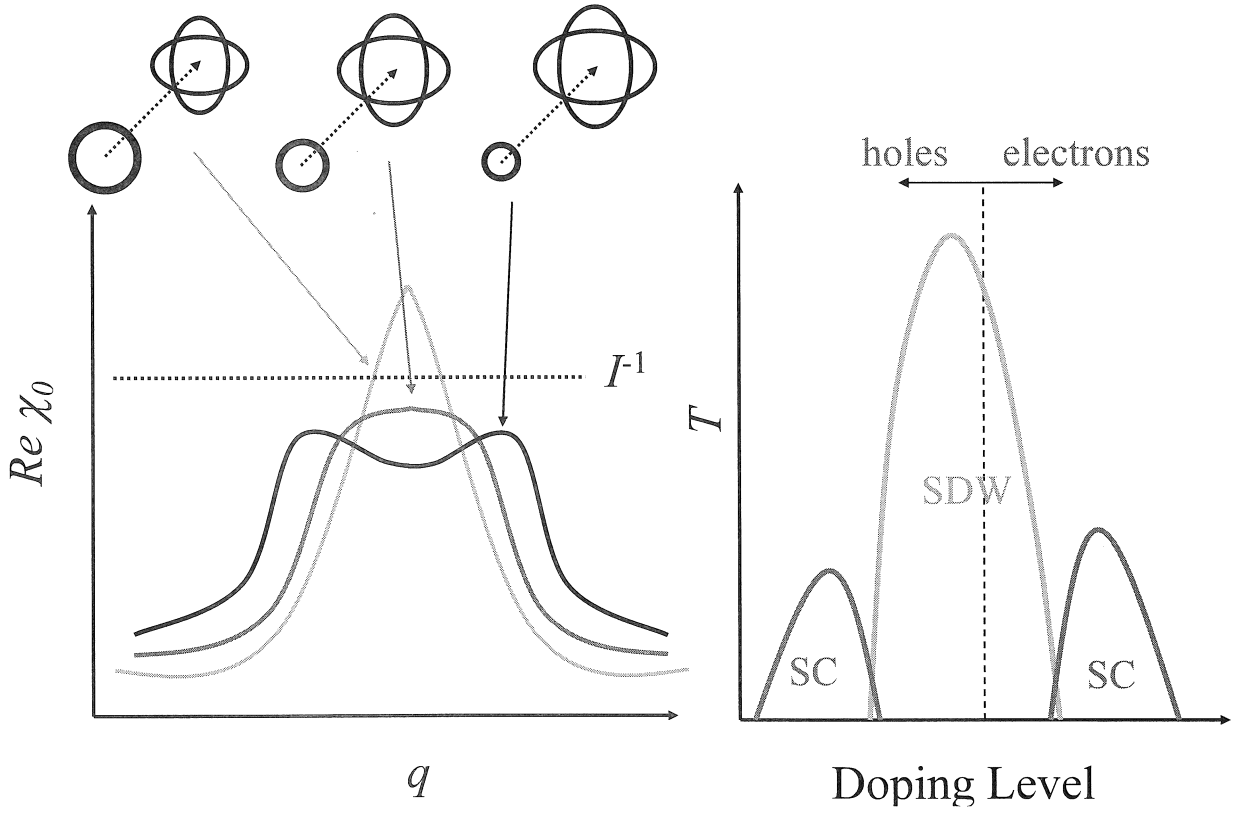

$Fe_{1+x}Te$

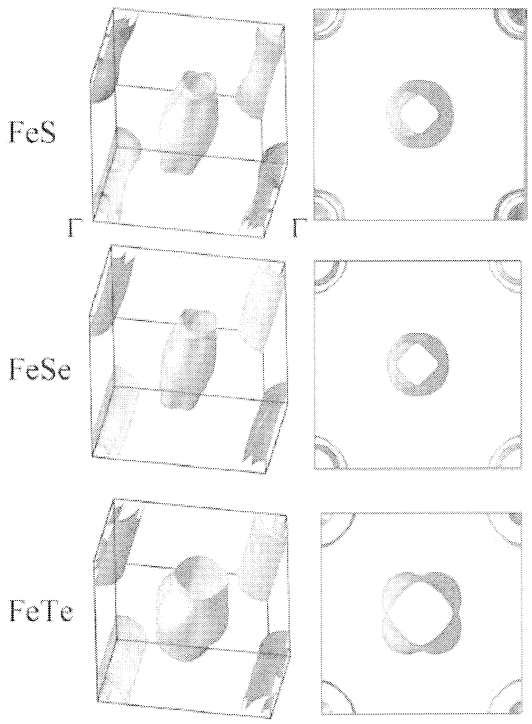

Subedi, et al., PRB (2008)

- $Fe_{1+x}Te$ has larger Fermi surface, greater tendency towards magnetism than the other compounds.
- Excess Fe is magnetic, and may also stabilize magnetism over fluctuating state. Excess Fe occurs as Fe^{1+} (Zhang).
- Experiment shows evolution as function of Fe doping from commensurate (not the same as FeSe) to incommensurate at high doping. Moments are large (~2 μ_B).
- May be useful to use another monovalent to dope (e.g. Tl) and replace excess Fe.

Comparison with Cuprates

	Cuprates	Fe-As
Magnetic & superconducting phases	Yes, magnetic phase insulating above & below T_N (Mott insulator)	Yes. Magnetic phase is metallic. Above T_N is is similar to the metal in the superconducting phase.
Electronic structure	Moderate $N(E_F)$, large FS at least for optimal doped	High $N(E_F)$, small disconnected FS
Doping	Essential.	Destruction of SDW is enough.
Magnetic character	Local moment	Strong coupled, apparently itinerant. Need neutron scattering.
Correlations	Strong. Mott-Hubbard type (e.g. p.e. satellites)	Probably strong but different e.g. spin fluctuations. Not Mott-Hubbard type.
Superconductivity	*d*-wave. Nodes. One band. Highly anistropic	Nodeless (*s* +/- ?). Two band. Maybe less anisotropic.
Structure	Oxides, corner shared octahedra -- complex	Simpler – tetragonal / orthorhombic, small unit cells.

Speculation Regarding Gap

Suppose that SDW-like pairing and superconductivity co-exist on the Fermi surface at different **k**.

This could be dependent on applied field, i.e. field could favor the magnetic state over the superconducting state.

Could then get superconducting gap on part of F.S. and magnetic pairing pseudogap on part of the F.S., with line nodes in between.

Cuprate pseudogap competes with superconductivity but coexists.

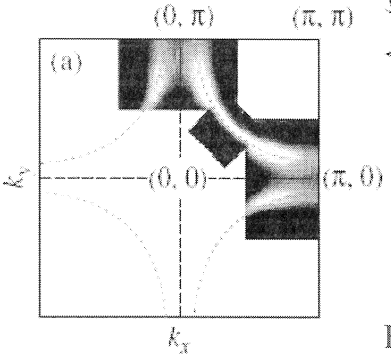

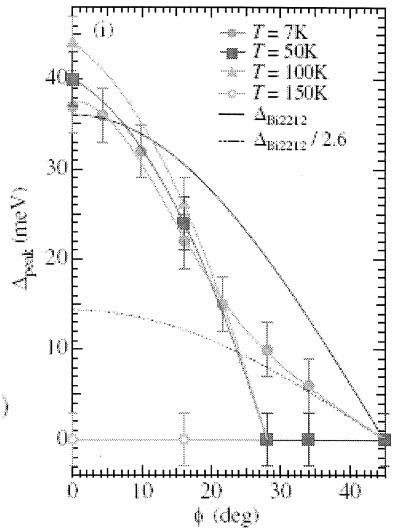

Bi-2201 Kondo, et al. (2007)

5. First-Principles Calculations of Crystal and Electronic Structures of LaFeAsO under Hydrostatic Pressure

Shoji Ishibashi[1,3], and Kiyoyuki Terakura[2]

[1]Research Institute for Computational Sciences (RICS), National Institute of Advanced Industrial Science and Technology (AIST), 1-1-1 Umezono, Tsukuba, Ibaraki 305-8568, Japan, [2]Research Center for Integrated Science (RCIS), Japan Advanced Institute of Science and Technology (JAIST), 1-1 Asahidai, Nomi, Ishikawa 923-1292, Japan, [3]JST, Transformative Research-Project on Iron Pnictides (TRIP), 5 Sanbancho, Chiyoda, Tokyo 102-0075, Japan

The discovery of the new superconductor $LaO_{1-x}F_xFeAs$ (Tc = 26 K) [1] is one of the strongest impact to the materials science community. So far, we have reported first-principles electronic-structure studies of a mother material LaFeAsO [2,3].

In the present study, by means of first-principles calculations with and without magnetic polarization, we have determined crystal structures of LaFeAsO under hydrostatic pressure and obtained electronic structures corresponding to them. Details of structural parameters and electronic density of states have been analyzed as a function of hydrostatic pressure. Effects of introduction of oxygen vacancies and substitution of Y for La have been also investigated.

References

[1] Y. Kamihara, T. Watanabe, M. Hirano and H. Hosono, J. Am. Chem Soc. **130**, 3296 (2008).

[2] S. Ishibashi, K. Terakura and H. Hosono, J. Phys. Soc. Jpn. **77**, 053709 (2008).

[3] S. Ishibashi and K. Terakura, Proc. Int. Symp. Fe-Pnictide Superconductors, J. Phys. Soc. Jpn. **77**, Suppl. C, pp. 91-95 (2008).

AIST

First-Principles Calculations of Crystal and Electronic Structures of LaFeAsO under Hydrostatic Pressure

Shoji Ishibashi[1,3], and Kiyoyuki Terakura[2]

[1]Research Institute for Computational Sciences (RICS),
National Institute of Advanced Industrial Science and Technology (AIST),
1-1-1 Umezono, Tsukuba, Ibaraki 305-8568, Japan

[2]Research Center for Integrated Science (RCIS),
Japan Advanced Institute of Science and Technology (JAIST),
1-1 Asahidai, Nomi, Ishikawa 923-1292, Japan

TRiP [3]JST, Transformative Research-Project on Iron Pnictides (TRIP),
5 Sanbancho, Chiyoda, Tokyo 102-0075, Japan

AIST

Summary of our previous results about a possible ground state and its electronic structure of LaFeAsO

S. Ishibashi, K. Terakura and H. Hosono: J. Phys. Soc. Jpn. 77, 053709 (2008).

S. Ishibashi and K. Terakura: J. Phys. Soc. Jpn. 77, (2008) Suppl. C, pp. 91.

NATIONAL INSTITUTE OF ADVANCED INDUSTRIAL SCIENCE AND TECHNOLOGY (AIST)

AIST

qmas_atom
a code for generating atomic wavefunctions, pseudo-wavefunctions, projector functions, a local potential, compensation charge functions.

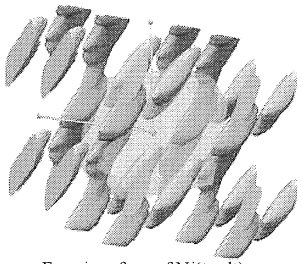

Fermi surface of $Ni(tmdt)_2$

QMAS

(Quantum MAterials Simulator)

S. Ishibashi, T. Tamura, S. Tanaka, M. Kohyama and K. Terakura

Ab initio computational code with PAW+LSDA/GGA

Dielectric function for alpha-quartz

qmas_band
a code for calculating electronic states and physical properties of solids.
stress/force, space group, Mulliken charge, Berry phase, static electric field, dielectric function, LSDA/GGA+U, positron state and annihilation parameter, Coulomb cut-off, energy and stress density, 1D-wannier function, permittivity profile.

qmas_gamma
Γ point real version for defect studies.
force, Mulliken charge, thermostat (velocity scaling or Nosé-Hoover), Hyperfine parameters, positron state and annihilation parameter.

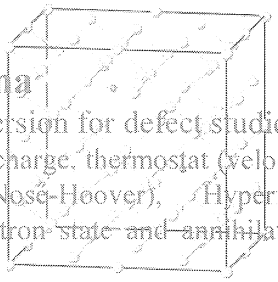

V-O complex in Si

NATIONAL INSTITUTE OF ADVANCED INDUSTRIAL SCIENCE AND TECHNOLOGY (AIST)

AIST

Computational conditions

- Planewave energy cutoff 20 hartree (+Pulay stress correction) or 30 hartree
- GGA(PBE96) + partial core correction
- ***k*** points 12 x 12 x 6, 10 x 10 x 6 and 6 x 6 x 6 in full BZ for 1x1, c(2x2) and 2x2 cells, respectively.
- Convergence criterion for atomic force 5 x 10^{-5} hartree/bohr
- Convergence criterion for stress 5 x 10^{-7} hartree/$bohr^3$

AIST

Reliability of our PAW calculation with reference to all-electron calculation

Note added. After submission of this paper, we became aware of a paper by Ishibashi *et al.*[41] These authors applied an in-house pseudopotential code to four different fully AFM patterns ($\mu \cong 1.8\ \mu_B$ on all sites). Their stabilization energies in all four cases agree with our all-electron results within 7 meV/f.u.

Mazin *et al.*, Phys. Rev. B **78**, 085104 (2008).

AIST

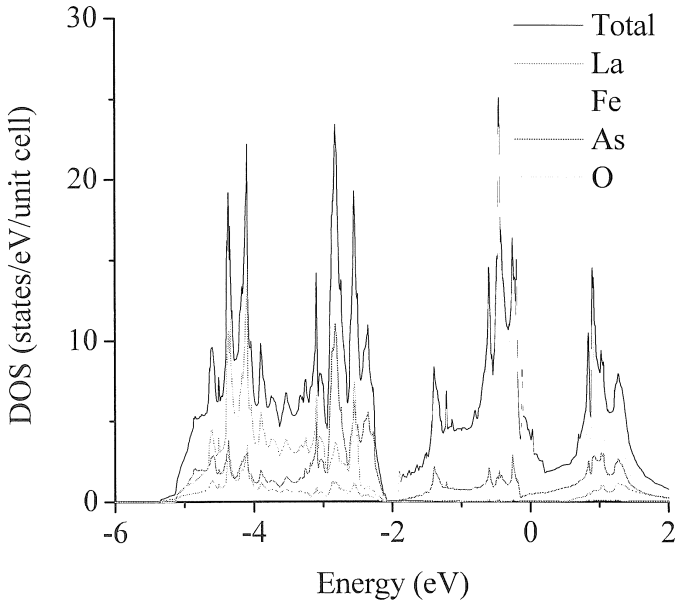

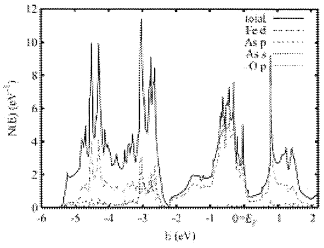

FIG. 1 (color online). LDA density of states and projections onto the LAPW spheres on a per formula unit both spins basis. Note that much of the As p character will be outside the As sphere, reducing their apparent weight.

cf. D. J. Singh and M.-H. Du: Phys. Rev. Lett. **100**, 237003 (2008).

DOS for the NM state of LaFeAsO with the experimental structure. The energy zero corresponds to the Fermi level.

NATIONAL INSTITUTE OF ADVANCED INDUSTRIAL SCIENCE AND TECHNOLOGY (AIST)

AIST

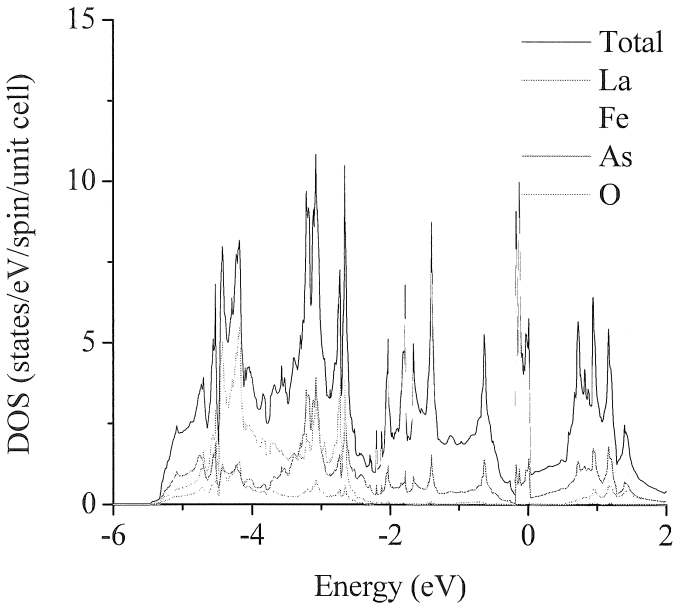

DOS for the AFM-G state of LaFeAsO with the experimental structure. The energy zero corresponds to the Fermi level.

AIST

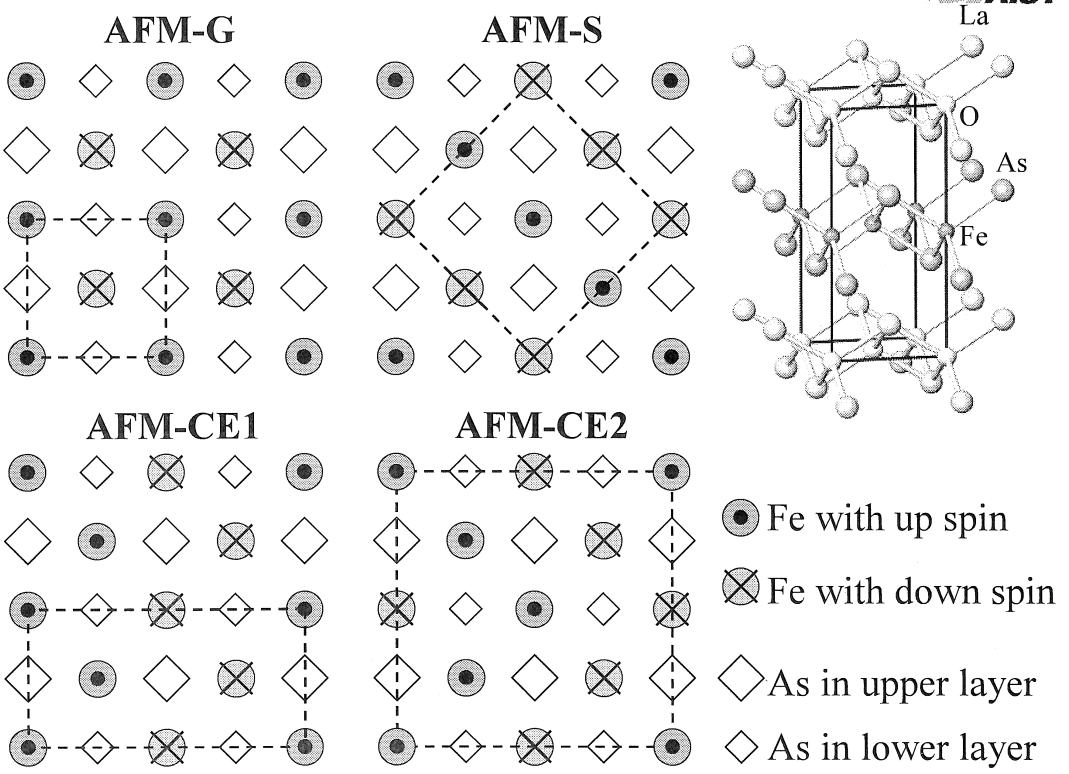

AIST

Magnetic stabilization energies and moments for LaFeAsO

Type	ΔE (eV/formula)	M (μ_B)	ΔE_{opt} (eV/formula)	M_{opt} (μ_B)
FM	-0.004	0.40	—	—
AFM-G	-0.080	1.89	-0.016	1.51
AFM-S	-0.174	2.12	-0.098	2.00
AFM-CE1	-0.064	1.88	—	—
AFM-CE2	-0.116	2.12	—	—

experimental structure at RT　　optimized structures

Experimental results
~0.35 μ_B
neutron, de la Cruz et al., arXiv:0804.0795
Mössbauer, Kitao et al., arXiv:0805.0041

AIST

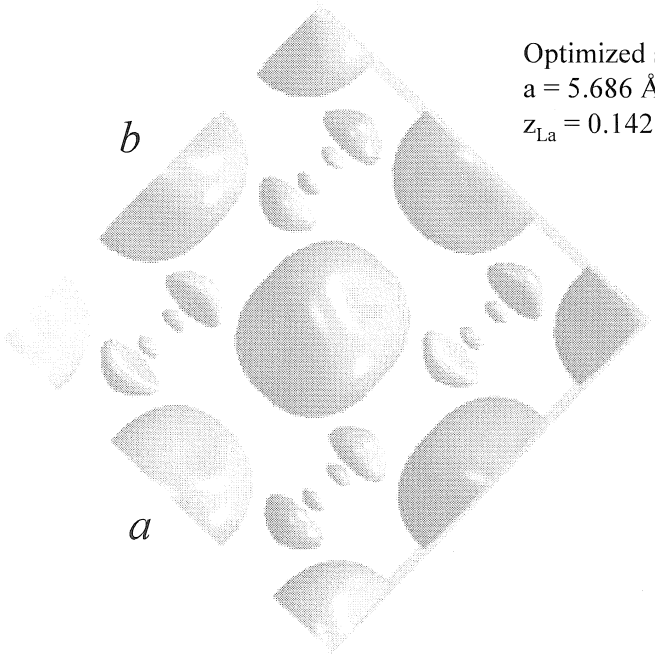

Optimized structural parameters
a = 5.686 Å, b = 5.758 Å, c =8.707 Å
z_{La} = 0.142, z_{As} = 0.646

Spin density distribution viewed along the c direction for the AFM-S state of LaFeAsO. Isodensity surface contours for the difference between the up-spin and down-spin electron densities are plotted. The blue and red surfaces correspond to 0.005 electrons/bohr^3, respectively.

NATIONAL INSTITUTE OF ADVANCED INDUSTRIAL SCIENCE AND TECHNOLOGY (AIST)

AIST

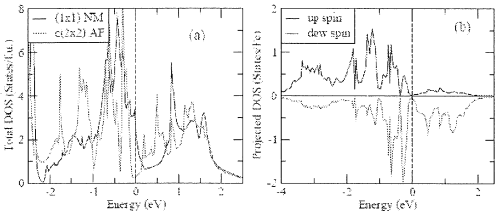

cf. J. Dong *et al.*:
condmat:0803.3426.

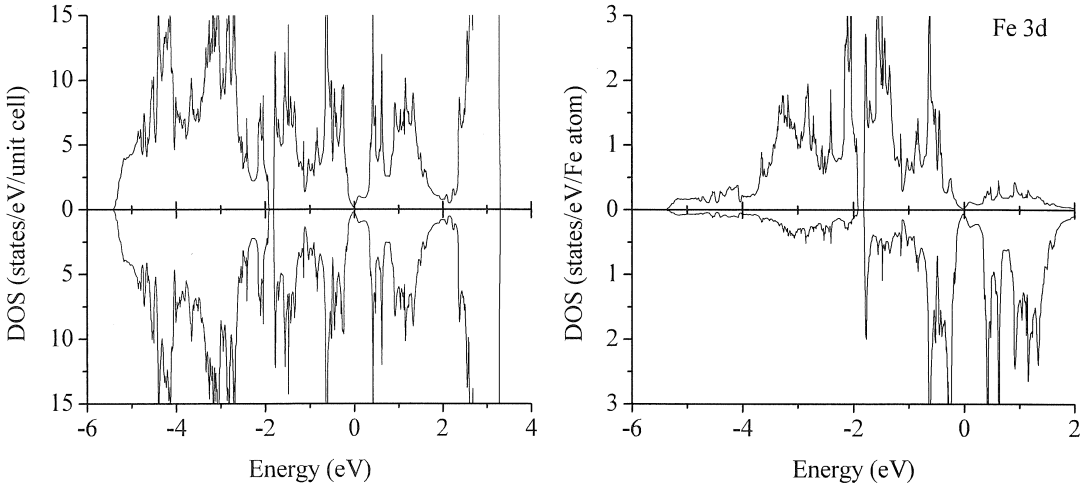

Total DOS (left) and Fe d partial DOS (right) for the AFM-S state of LaFeAsO

AIST

Optimized crystal structures and comparison with experimental ones

Type	a (Å)	b (Å)	c (Å)	z_{La}	z_{As}
NM	4.0132 (5.6755)		8.6447	0.1450	0.6392
AFM-G	4.0407 (5.7144)		8.6431	0.1434	0.6420
AFM-S	5.6857	5.7578	8.7070	0.1425	0.6464
Exp. (RT)*	4.0353 (5.7068)		8.7409	0.1415	0.6512
Exp. (120 K)**	5.6826	5.7104	8.7196	0.1417	0.6513

*Y. Kamihara, T. Watanabe, M. Hirano and H. Hosono: J. Am. Chem Soc. **130** (2008) 3296.

**T. Nomura, S. W. Kim, Y. Kamihara, M. Hirano, P. V. Sushko, K. Kato, M. Takata, A. L. Shluger and H. Hosono: arXiv:0804.3569.

AIST

Hydrostatic pressure

AIST

Backgrounds

- Calculated Fe magnetic moment is sensitive to Fe-As distance.

  cf. Yin *et al.*: Phys. Rev. Lett. **101**, 047001 (2008).

- Tc seems sensitive to As-Fe-As angle.

  cf. Lee *et al.*: J. Phys. Soc. Jpn. **77**, 083704 (2008).

Hydrostatic pressure can change the Fe-As distance and As-Fe-As angle on one material.

- Experimental report start to appear.

  cf. Kumai *et al.*: J. Phys. Soc. Jpn. **78**, 013705 (2009).

AIST

Figures and values in this part will be published elsewhere.

AIST

Summary

- Our calculation predicts that the ground state of LaFeAsO is **antiferromagnetic with a stripe-type** magnetic moment alignment (AFM-S) leading to orthorhombic symmetry of the crystal. In this particular magnetic state, the density of states at the Fermi level is very small. (LaFePO has turned out to be paramagnetic and a good metal.) The structural parameters have been successfully obtained for the magnetic calculation but there is a significant discrepancy in **the Fe magnetic moment (2.0 μ_B (calc.) vs. 0.35 μ_B (exp.))**.
- At zero pressure, the AFM-S cell is significantly larger than the NM cell. **The AFM structure is closer to the experimental structure** in spite of the discrepancy of the Fe magnetic moment. Under hydrostatic pressure, it is clearly shown **the system is much softer along the *c* direction**.
- Introduction of **oxygen vacancy** and **substitution of Y** for La do not affect significantly the compressibility along the *a* axis while do **affect the compressibility along the *c* axis**.

NATIONAL INSTITUTE OF ADVANCED INDUSTRIAL SCIENCE AND TECHNOLOGY (AIST)

6. First-Principles GW Study of LaFeAsO: Electronic Structure and Correlation Effects

Takashi Miyake[1,3] and Ryotaro Arita[2,3]

[1]Research Institute for Computational Sciences, AIST, Tsukuba 305-8568, Japan
[2]Department of Applied Physics, University of Tokyo, Tokyo 113-8656, Japan
[3]Japan Science and Technology Agency, TRIP

Electron correlation effects in LaFeAsO are discussed based on first-principles calculations. Starting from the bandstructure obtained by density functional theory (DFT), we estimate the strength of the local interaction for the Fe 3d orbitals in the constrained random-phase-approximation (cRPA) combined with the maximally localized Wannier function [1,2]. For the "d model" where the model Hamiltonian is constructed from the manifold of the d states only, the value of Hubbard U is 2.2-3.4 eV depending on the orbital, with the largest (smallest) value for dxy (dx^2-y^2), and is 2.9 eV on average. The value is slightly smaller than that of bcc-Fe and significantly smaller than that of transition metal monoxides. The U parameter increases to 4.7 eV for the "dpp model" in which O 2p and As 4p states are also included in the model.

We also calculate the electron self-energy in the GW approximation. The shape of the GW bandstructure is similar to the DFT bandstructure, but the self-energy correction reduces the d bandwidth significantly by about 20 %. The real part of the self-energy monotonically decreases as a function of energy in [-5eV:5eV]. The renormalization factor (Z-factor) evaluated from the slope of the self-energy yields 0.5-0.7 and the value gets smaller near the Fermi level. More details will be given in the presentation.

References

[1] K. Nakamura, R. Arita and M. Imada, J. Phys. Soc. Jpn. **77**, 093711 (2008).
[2] T. Miyake, L. Pourovskii, V. Vildosola, S. Biermann and A. Georges, J. Phys. Soc. Jpn. **77**, Suppl. C, 99 (2008).

IRiSes2009
JAEA, Tokyo
Jan.25, 2009

First-principles GW study of LaFeAsO:
Electronic structure and correlation effects

RICS-AIST, Tsukuba, Japan[1]
Dept. of Applied Physics, Univ. of Tokyo, Japan[2]
JST-TRIP[3]
Takashi MIYAKE[1,3] and Ryotaro ARITA[2,3]

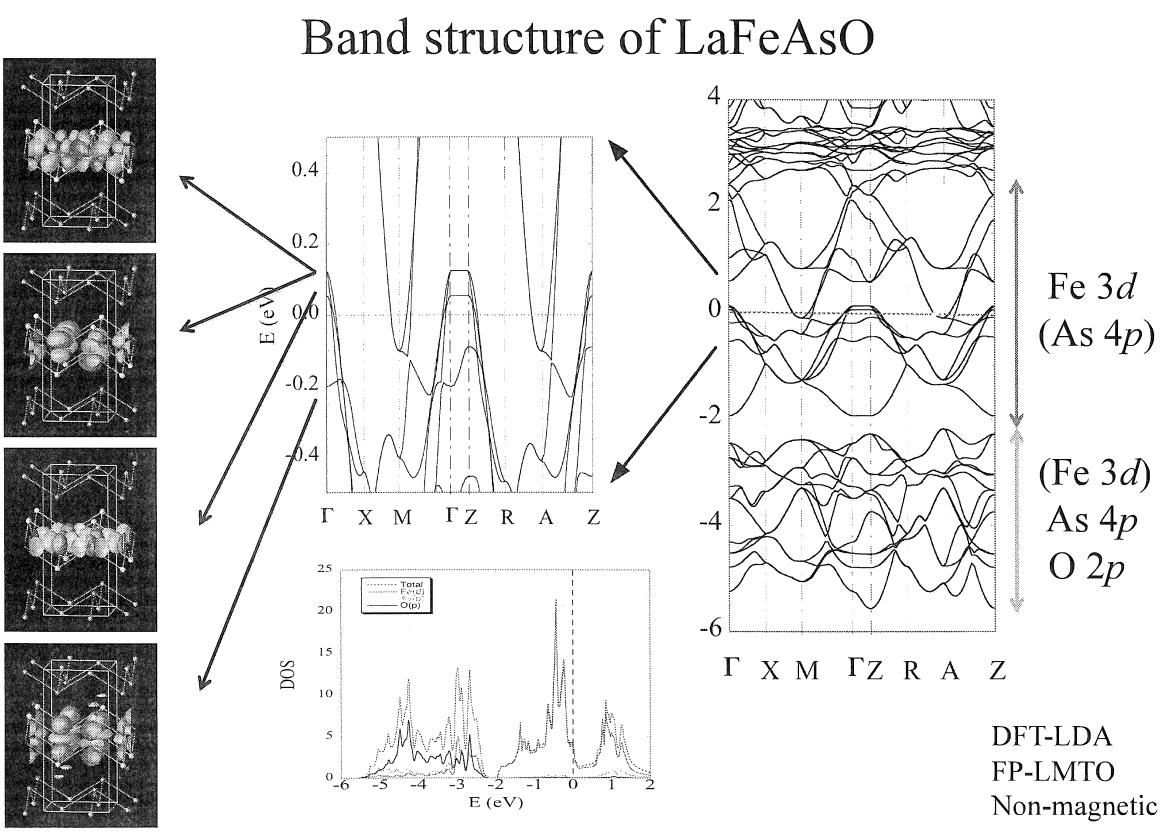

Maximally Localized Wannier Function

N. Marzari and D. Vanderbilt, PRB**56**, 12847 (1997)

I. Souza, N. Marzari and D. Vanderbilt, PRB**65**, 035109 (2001)

$$\psi_{n\mathbf{k}}^{(\mathrm{W})}(\mathbf{r}) = \sum_{m=1}^{\mathcal{N}_{\mathrm{k}}} \mathcal{U}_{mn}(\mathbf{k})\psi_{m\mathbf{k}}(\mathbf{r})$$

$$\varphi_{n\mathbf{R}}(\mathbf{r}) = \frac{1}{N}\sum_{\mathbf{k}} e^{-i\mathbf{k}\cdot\mathbf{R}}\psi_{n\mathbf{k}}^{(\mathrm{W})}(\mathbf{r})$$

xy *yz* $3z^2$-r^2 *xz* x^2-y^2

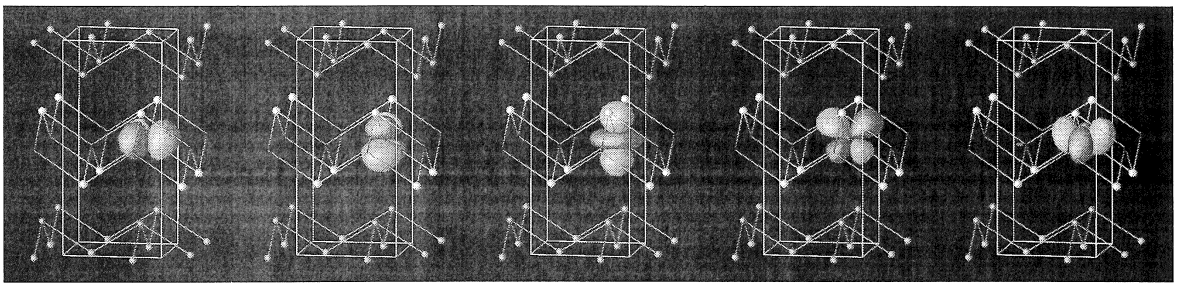

Constrained RPA

F.Aryasetiawan et al., Phys. Rev. B **70,** 195104 (2004)

TM and F.Aryasetiawan, Phys. Rev. B **77,** 085122 (2008)

$$U_{mn} = \langle \varphi_{m0}(\mathbf{r})\varphi_{m0}(\mathbf{r}) | W(\mathbf{r}, \mathbf{r}'; \omega = 0) | \varphi_{n0}(\mathbf{r}')\varphi_{n0}(\mathbf{r}') \rangle$$

$$W = \epsilon^{-1} v = \frac{v}{1 - vP}$$

$$P(\mathbf{r}, \mathbf{r}'; \omega) = \sum_{m}^{\mathrm{occ}} \sum_{n}^{\mathrm{unocc}} \psi_m(\mathbf{r})\psi_n^*(\mathbf{r})\psi_m^*(\mathbf{r}')\psi_n(\mathbf{r}') \times \left\{ \frac{1}{\omega - \epsilon_n + \epsilon_m + i\delta} - \frac{1}{\omega + \epsilon_n - \epsilon_m - i\delta} \right\}$$

$$\sum_{m}^{\mathrm{occ}} \sum_{n}^{\mathrm{unocc}} = \sum_{r}^{\mathrm{occ}} \sum_{r}^{\mathrm{unocc}} + \sum_{r}^{\mathrm{occ}} \sum_{d}^{\mathrm{unocc}} + \sum_{d}^{\mathrm{occ}} \sum_{r}^{\mathrm{unocc}} + \cancel{\sum_{d}^{\mathrm{occ}} \sum_{d}^{\mathrm{unocc}}}$$

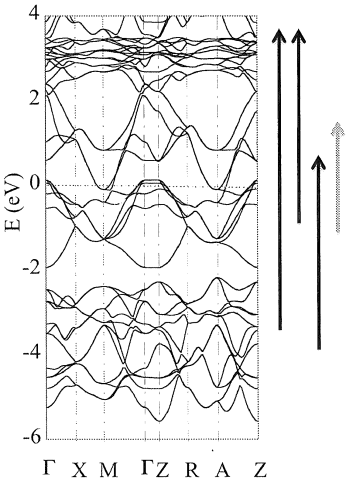

Effective Coulomb interaction (in eV)

c.f. K.Nakamura, R.Arita and M.Imada, J.Pys.Soc.Jpn.77, 093711(2008).
TM et al., J.Phys.Soc.Jpn.77 Suppl.C99(2008).

	xy	yz	$3z^2$-r^2	xz	x^2-y^2
xy	3.35	2.03	2.02	2.03	2.15
yz	2.03	2.76	2.25	1.85	1.73
$3z^2$-r^2	2.02	2.25	3.26	2.25	1.73
xz	2.03	1.85	2.25	2.76	1.73
x^2-y^2	2.15	1.73	1.73	1.73	2.18

U_{nn} = 2.2 - 3.4
$< U_{nn} >$ = 2.9
$< v_{nn} >$ = 13.1-18.2
$< J_{nm} >$ = 0.4
$< U_{nn} >$ = 0.7 (offsite)

xy yz $3z^2$-r^2 xz x^2-y^2

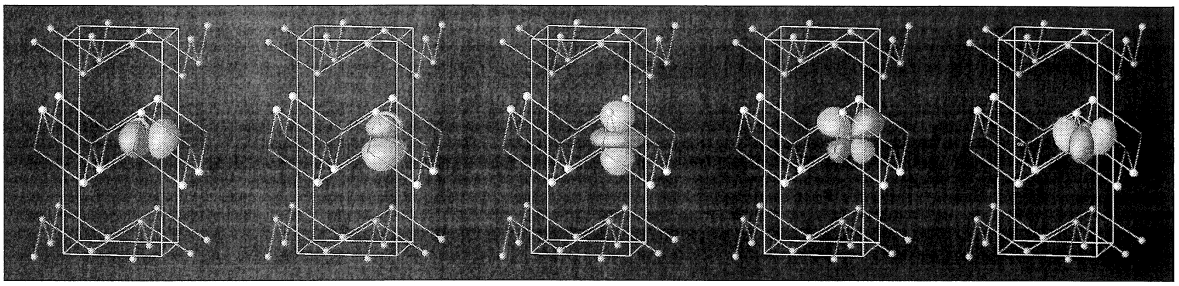

d-model vs. *dpp*-model

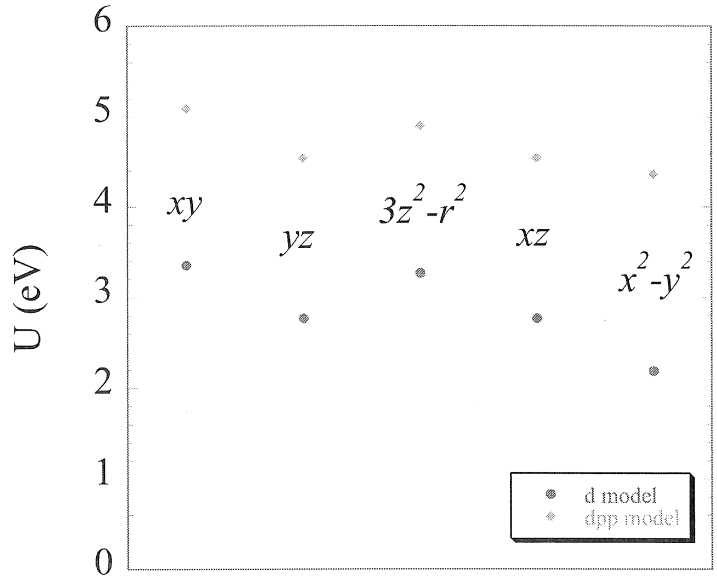

dpp-model
$< U_{dd} >$ = 4.8 (Fe)
$< U_{pd} >$ = 1.2 (Fe-As)
$< U_{pp} >$ = 2.9 (As-As)

d-model
$< U_{dd} >$ = 2.9

Ab-initio GW quasiparticle bandstructure

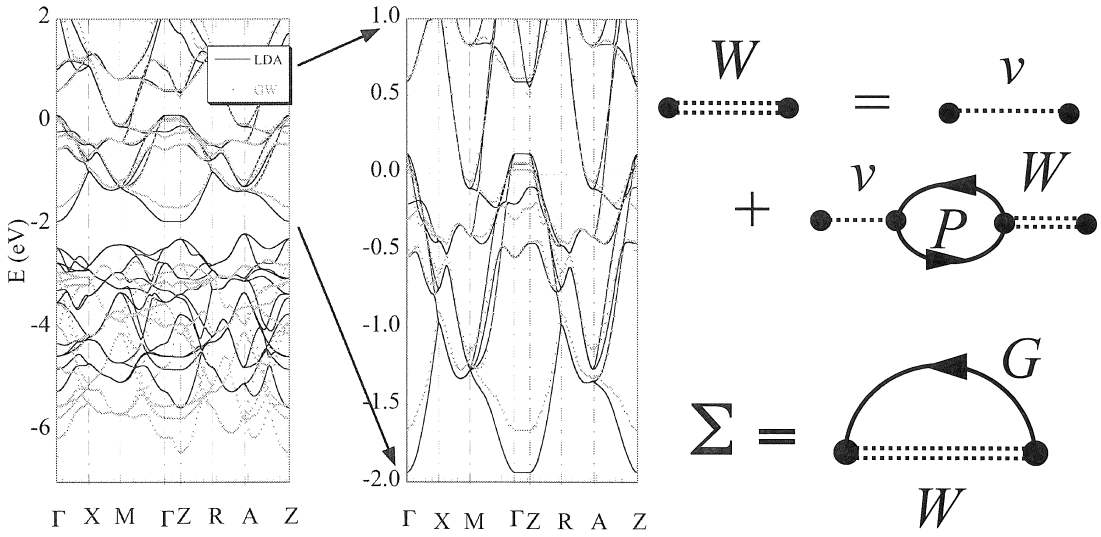

$$E_{\mathrm{k}n} = \epsilon_{\mathrm{k}n} + \langle \psi_{\mathrm{k}n} | \Sigma(E_{\mathrm{k}n}) - v_{\mathrm{xc}} | \psi_{\mathrm{k}n} \rangle$$

Self-energy and the Z-factor

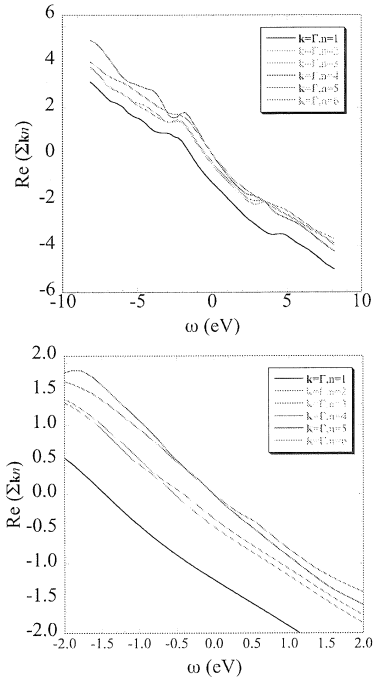

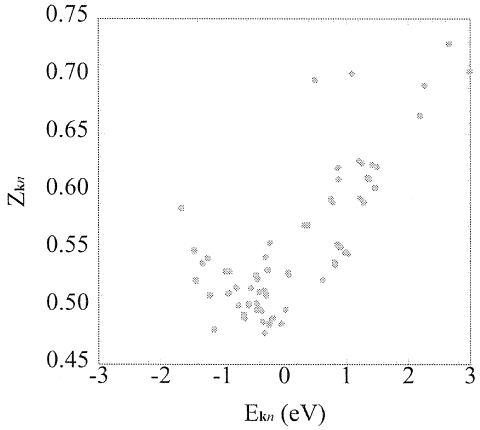

$$Z_{\mathrm{k}n} = \partial \Sigma^{\mathrm{r}}_{\mathrm{k}n}(\omega) / \partial \omega |_{\omega = \epsilon_{\mathrm{k}n}}$$

$$\Sigma^{\mathrm{r}}_{\mathrm{k}n}(\omega) = \mathrm{Re} \langle \psi_{\mathrm{k}n} | \Sigma(\omega) | \psi_{\mathrm{k}n} \rangle$$

Summary

- Moderately correlated system with orbital dependent U
  U_{dd} =2.2-3.4 eV, $U/t \sim 10$ in the *d*-model

- Orbital dependence is weaker in the *dpp*-model
  U_{dd} =4.4-5.1 eV

- GW self-energy correction decreases the *d* band width,
  while it pushes down and widen the *p* band.

- The self-energy is a smooth function of frequency.
  Z = 0.5-0.6 near the Fermi level

- (*Preliminary*) the GW self-energy suppresses magnetic instability
  at the M point.

7. ±s-wave Scenario in Iron-based Superconductors: Thermodynamics and Josephson Effects

M. Machida[1,3], Y. Nagai[2,3], Y. Ohta[1], H. Nakamura[1,3], N. Nakai[1], M.Okumura[1], and N. Hayashi[1]

[1]Center for Computational Science & e-Systems, Japan Atomic Energy Agency, Tokyo 110-0015, Japan & CREST(JST) Saitama, 332-0012, Japan
[2]Department of Physics, University of Tokyo, Tokyo 113-0033, Japan
[3]JST, TRIP, Tokyo 102-0075, Japan

Since the discovery of new high-Tc superconductivity in $LaFeAsO_{1-x}F_x$ [1], a tremendous number of studies on the materials have been uploaded on arXiv cond-mat and published. Among them, one of the most important issues is to identify Cooper pair symmetry, because the symmetry is deeply related to the superconductivity mechanism and crucial in designing the future application. So far, the ±s-wave pairing symmetry has been theoretically proposed as one of the candidates of the pairing symmetry in Fe-pnictide superconductors [2]. The ±s-wave symmetry means that the symmetry of pair functions on each Fermi surface is s-wave and the relative phase between them is π. In this paper, we firstly clarify that the ±s-wave symmetry explains the lack of the coherence peak and the low temperature power-law behavior in the nuclear magnetic relaxation rate with an assumed gap anisotropy [3]. This is consistent with the data of the temperature dependence of the penetration depth. Secondly, we show that the symmetry brings about a drastic and rich physics in the Josephson junction to the single-band superconductors [4]. The theory exhibits that the critical current, the Fraunhofer pattern, I-V characteristics etc. are drastically changed when the two s-wave gap amplitude is equal [4].

References

[1] Kamihara Y, Watanabe T, Hirano M and Hosono H 2008 *J. Am. Chem. Soc.* **130** 3296.
[2] See, e.g., Mazin I I, Singh D J, Johannes M D and Du M H 2008 *Phys. Rev. Lett.* **101** 057003 & Kuroki K, Onari S, Arita R, Usui H, Tanaka Y, Kontani H and Aoki H 2008 *Phys. Rev. Lett.* **101** 087004C.
[3] Y.Nagai, N.Hayashi, N.Nakai, H.Nakamura, M.Okumura, and M.Machida, New J. of Phys. 10 (2008) 103026.
[4] Y.Ota, Y.Nagai, N.Hayashi, N.Nakai, H.Nakamura, M.Okumura, and M.Machida, (in Preparation).

±s-wave Scenario in Iron-based Superconductors: Thermodynamics and Josephson Effects

Masahiko Machida[a,b,c]

Yukihiro Ohta[a,b], **Tomio Koyama**[b,d]
Yuki Nagai[c,e], **Nobuhiko Hayashi**[a,b]
Hiroki Nakamura[a,c], **Noriyuki Nakai**[a,b]

[a]CCSE, Japan Atomic Energy Agency
[b]CREST (JST) & [c]TRIP (JST)
[d]Institute for Material Research, Tokoku University
[e]Tokyo University

Outline

1、Introduction

Superconducting
Fe-based Layered Compounds

Y. Kamihara, *et al.*, J. Am. Chem. Soc. 128, 10012 (2006);
H. Takahashi, *et al.*, Nature 452, 376 (2008)

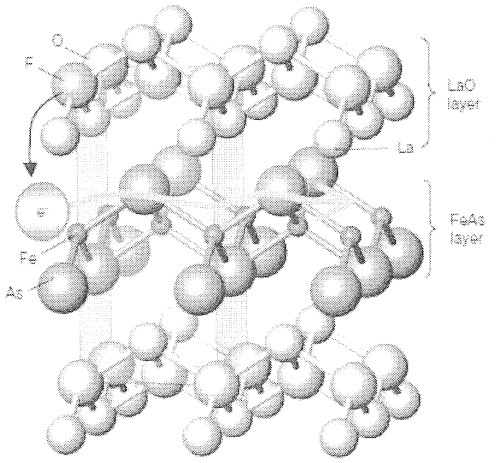

Figure 1 | **Schematic crystal structure of LaOFeAs.** Electron carriers generated by F-doping into oxygen sites are injected into FeAs metallic layers as a result of the large energy offset between these two layers. We note that the carrier doping layer is spatially separated from the conduction layer.

Tc = 43 K

Multi-Gap Superconductor

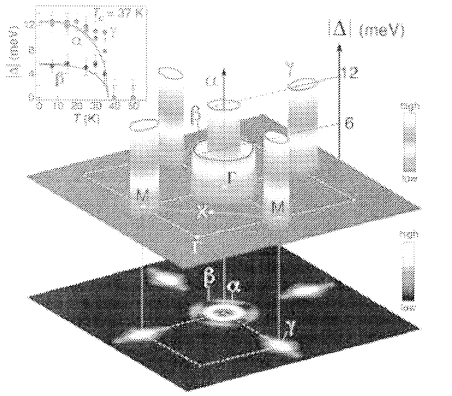

Fig. 4: (Colour on-line) Three-dimensional plot of the superconducting-gap size (Δ) measured at 15 K on the three observed FS sheets (shown at the bottom as an intensity plot) and their temperature evolutions (inset).

Introduction

Superconducting
Fe-based layered compounds

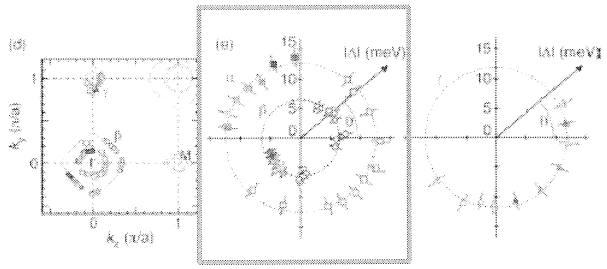

H. Ding, *et al.*, Euro. Phys. Lett. 83, 47001 (2008)

$Ba_{0.6}K_{0.4}Fe_2As_2$

Experimental Evidence for Two Gaps

2, A Scenario to Resolve the Controversy between NMR & Other Exp.

NMR 1/T_1

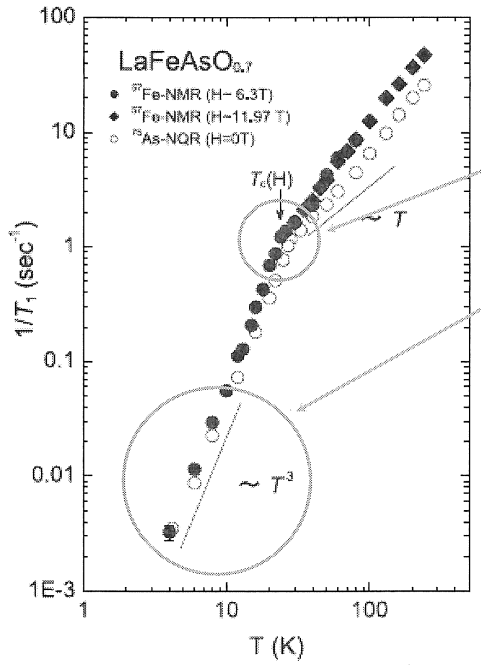

Terasaki et al.,arXiv:0809.5155

NMR 1/T_1

DOS^2 + Coherence

No Coherence Peak

Power Law Decay

Nodal Gap

Anisotropic ±S wave

2, A Scenario to Resolve the Controversy between NMR & Other Exp.

Superfluid Density

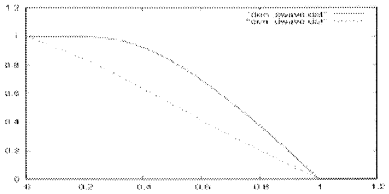

LaFeAs($O_{1-x}F_x$)

Luetkens et al.,arXiv:0806.3533

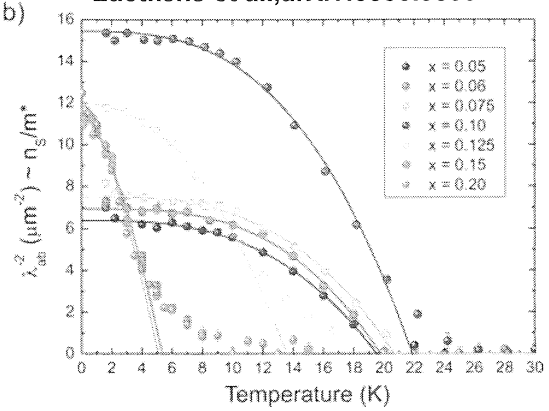

PrFeAsO_{1-y}

Hashimoto et al.,arXiv:0806.3149

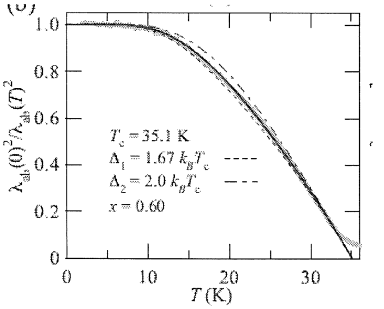

LaFeAs($O_{1-x}F_x$)

Takeshita et al.JPSJ 77 (2008) 103703

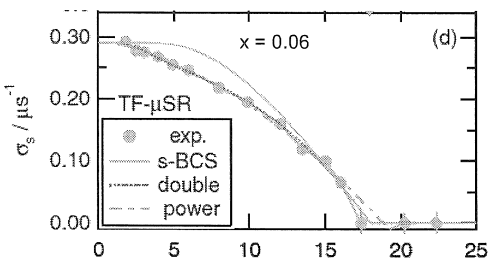

Full Gap

vs.

Line Node

2, A Scenario to Resolve the Controversy between NMR & Other Exp.

NMR $1/T_1$: How to Eliminate a Coherence Peak Just on T_c

$$f_{\uparrow\downarrow}(k_F, i\omega_n) = \frac{\Delta(k_F)}{\sqrt{\omega_n^2 + |\Delta(k_F)|^2}},$$

Line Integral Δ on Fermi-surface

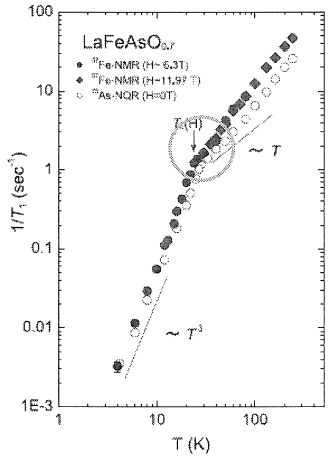

Terasaki et al.,arXiv:0809.5155

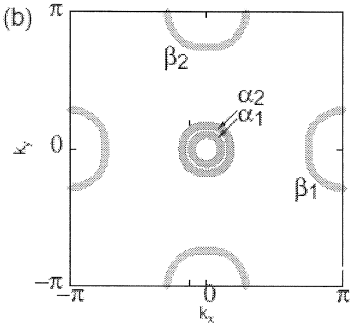

±s-wave scenario cancels the coherence peak

2, A Scenario to Resolve the Controversy between NMR & Other Exp.

NMR $1/T_1$: How to Obtain T^3 far below T_c

$$g_{\uparrow\uparrow}(k_F, i\omega_n) = \frac{\omega_n}{\sqrt{\omega_n^2 + |\Delta(k_F)|^2}},$$

A Linear Like DOS

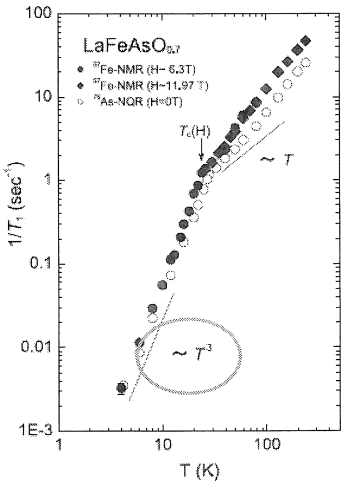

Terasaki et al.,arXiv:0809.5155

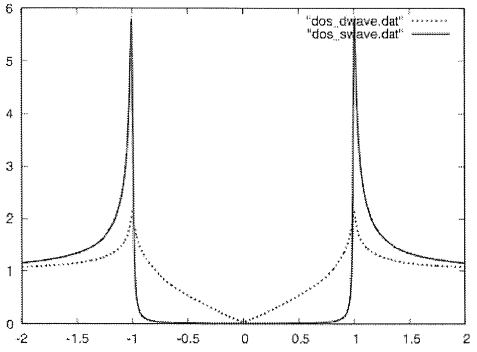

Anisotropic S-wave Scenario

(Impurity Scenario)

2, A Scenario to Resolve the Controversy between NMR & Other Exp.

Anisotropy ±S wave

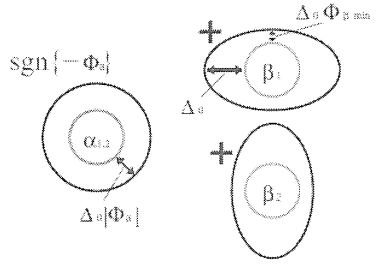

NMR $1/T_1$

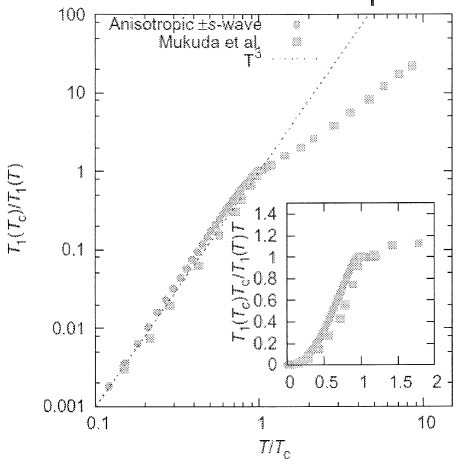

Kuroki et al.,PRL 101(2008) 147003

Superfluid Density

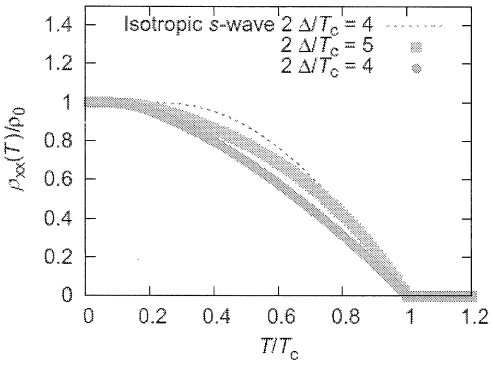

Anisotropic ±S wave scenario explains exp.

Y.Nagai et al, New J. Phys. **10** (2008) 103026

3, How to Detect ±s-wave using Josephson Effects

High-T_c Cuprate Superconductors

Tri-crystal Junction
Half Quantized Vortex

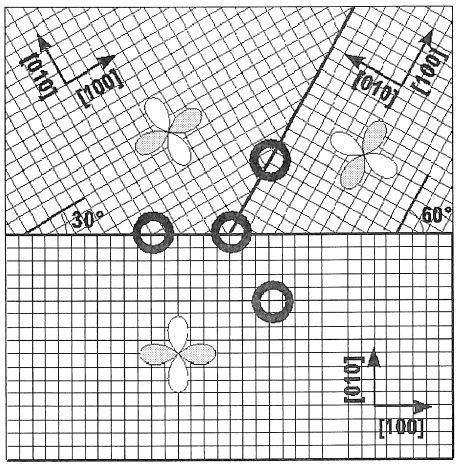

High-T_c Fe-based Superconductors

Josephson Junction (SIS)

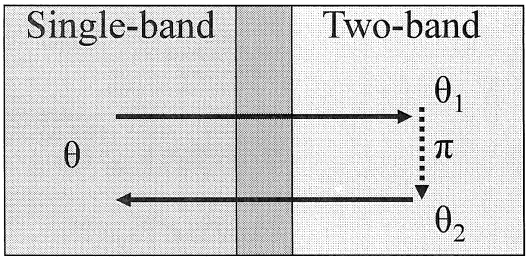

T.K.Ng, & N.Nagaosa
D.Inotani & Y.Ohashi

3, How to Detect ±s-wave using Josephson Effects

Simple Microscopic Theory

Hamiltonian

S.G. Sharapov, *et al.*, Eur. Phys. J. B 30, 45 (2002)

$$\mathcal{H}_{\rm pair} = -g_1\hat{\psi}^\dagger_\uparrow\hat{\psi}^\dagger_\downarrow\hat{\psi}_\downarrow\hat{\psi}_\uparrow - g_2\hat{\varphi}^\dagger_\uparrow\hat{\varphi}^\dagger_\downarrow\hat{\varphi}_\downarrow\hat{\varphi}_\uparrow - g_{12}(\hat{\psi}^\dagger_\uparrow\hat{\psi}^\dagger_\downarrow\hat{\varphi}_\downarrow\hat{\varphi}_\uparrow + \text{h.c.})$$

1st band　　2nd band　　inter-band pairing

mean field approximation ⇒

$$\frac{g_2}{g}|\Delta_1|^2 + \frac{g_1}{g}|\Delta_2|^2 - \frac{g_{12}}{g}(\Delta_1^*\Delta_2 + \text{c.c.})$$

$$g = g_1g_2 - g_{12}^2$$

$g_{12} > 0$ (attractive inter-band coupling) ⇒ $J_{\rm in} > 0$ **0-shift**

$g_{12} < 0$ (repulsive inter-band coupling) ⇒ $J_{\rm in} < 0$ **π-shift**

$$\frac{\hbar J_{\rm in}}{e^*}\cos(\varphi_l^{(1)} - \varphi_l^{(2)})$$

Inter-band Josephson coupling energy

3, How to Detect ±s-wave using Josephson Effects

Physical Analogy

$$\mathcal{L}_{\rm eff} = \frac{s_{\rm L}}{8\pi\mu^2}\left(A_{\rm L}^0 + \frac{\hbar}{e^*}\partial_t\varphi_{\rm s}\right)^2 + \sum_{l=1}^{2}\frac{s_{\rm R}}{8\pi\mu_l^2}\left(A_{\rm R}^0 + \frac{\hbar}{e^*}\partial_t\varphi^{(l)}\right)^2$$

$$-\frac{s_{\rm L}}{8\pi\lambda^2}\left(\frac{\hbar c}{e^*}\partial_x\varphi_{\rm s} - A_{\rm L}^x\right)^2 - \sum_{l=1}^{2}\frac{s_{\rm R}}{8\pi\lambda^{(l)\,2}}\left(\frac{\hbar c}{e^*}\partial_x\varphi^{(l)} - A_{\rm R}^x\right)^2$$

$$+\frac{hj_1}{e^*}\cos\theta^{(1)} + \frac{hj_2}{e^*}\cos\theta^{(2)} + \frac{hJ_{\rm in}}{e^*}\cos(\varphi^{(1)} - \varphi^{(2)}) + \frac{\epsilon d}{8\pi}E_{\rm RL}^{z\,2} - \frac{d}{8\pi}B_{\rm RL}^{y\,2}$$

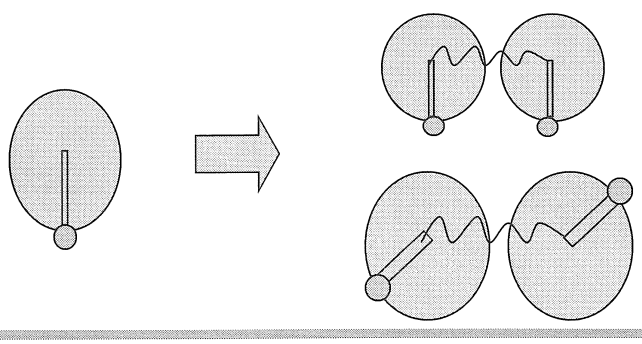

++S-wave

Coupled Oscillator

±S-wave

3, How to Detect ±s-wave using Josephson Effects

Eigen-modes in Josephson Junction (SIS)

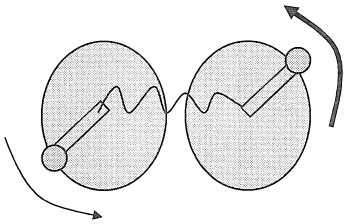

Josephson Plasma Mode（in-phase)

++ S-wave: $\Omega \sim \omega_{p1} + \omega_{p2}$

+− S-wave: $\Omega \sim \omega_{p1} - \omega_{p2}$

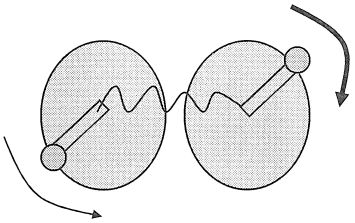

Josephson Leggett's Mode（Out-of-phase)

++ S-wave: } $4\bar{\alpha}\nu_{12}^2$ $\nu_{12}^2 \propto J_{in}$

+− S-wave: }

MgB_2 Bulk-Leggett's mode PRL(2007)

3, How to Detect ±s-wave using Josephson Effects

Fraunhofer diffraction pattern in Josephson Junction (SIS)

$$\varphi = \pi \qquad I(H^y, \theta_0) = L_x \sin(\theta^0 + \bar{\eta}\pi/\eta_2) \left[(j_1 - j_2) \frac{2}{kL_x} \sin \frac{kL_x}{2} \right]$$

when $j_1 = j_2$ ⟶ diffraction pattern completely disappears

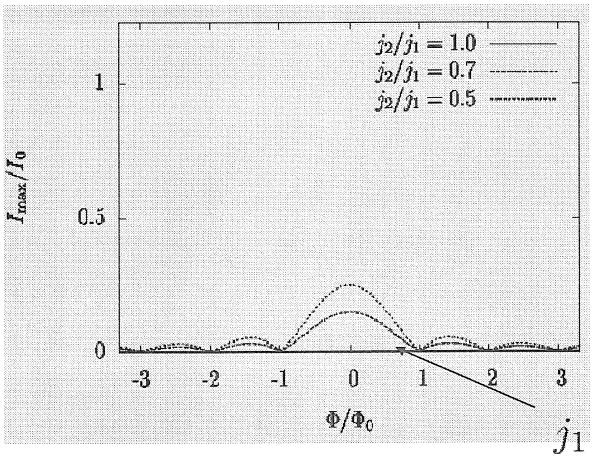

$j_1 = j_2$

The maximum value drastically small

``Diffraction Cancel"

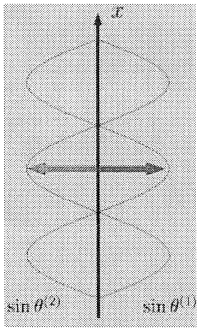

4, Summary & Conclusion

1, Anisotropic ±s-wave scenario well explains both **NMR & superfluid density**.

2, ±s-wave scenario predicts **anomalous Josephson effects** in S(2-band)IS(1-band) Junction

8. Investigation of Superconductivity in Iron-Selenide with Single Crystals and Epitaxial Thin Films

Maw-Kuen Wu
Institute of Physics, Academia Sinica, Taipei Taiwan

In order to gain more insight into the origin of superconductivity in the infinite-layer $Fe_{1+x}Se$ system, we have developed processes to grow single crystals and epitaxial thin films. Single crystals of nominal composition $Fe_{1.14}Se$ and $Fe_{1.18}SeMn_{0.1}$ have been grown from KCl solutions. Crystals measuring 2-3 mm across and 0.1-0.3 mm thick grow with hexagonal plate like habit. Powder x-ray diffraction (XRD) measurements show that the plate side of the crystal is along the (101) face of the tetragonal α-FeSe. The as grown crystals show a superconducting transition T_c at 8 K from both DC magnetization and resistive measurements. Specific heat measurements also confirm bulk superconductivity in these crystals. On the other hand α-phase $Fe_{1+x}(Se_{1-y}Te_y)$ thin films have been fabricated by pulsed laser deposition on MgO substrate. All $Fe_{1+x}(Se_{1-y}Te_y)$ films have c-axis preferred orientation and smooth surface morphology. Based on the energy-dispersive X-ray (EDX) chemical analysis, the as grown films reveal Se-rich characteristic. The superconducting transition temperatures of films are suppressed, in comparison with the bulk samples, which can be attributed to Se-rich and the substrate effect. More detailed studies with 3d transition metals doping on the crystals $(T_{M0.1}Fe_{0.9})_{1.18}Se$ show that Mn-doping does not affect superconductivity, whereas Cu-doping completely suppresses superconductivity. Detailed x-ray structural studies support that the existence of a low temperature structural distortion in this class of material is essential for the occurrence of superconductivity.

Investigation of Superconductivity in Iron-Selenide with Single Crystals and Epitaxial Thin Films

M. K. Wu
Institute of Physics, Academia Sinica
Taipei, Taiwan

Present at IRiSes2009
January 25, 2009
Tokyo, Japan

OUTLINE

- Single Crystal Growth of α – FeSe
- Fabrication of α – FeSe(Te) Thin Films
- Some properties of FeSe Superconductor
  - Transport properties
  - Magnetic properties
  - Specific heat
  - Structural Instability and Superconductivity
- Summary

FeSe system

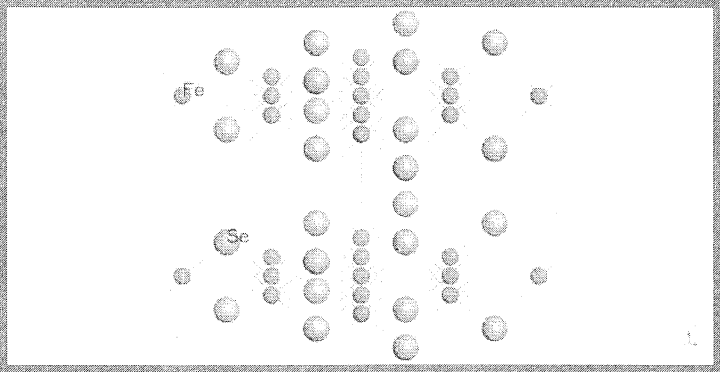

Structure type: B10, anti-PbO
Pearson symbol: tP4
Space group: P4/nmm, No. 129
a= 3.783, C=,5.534
Fe 2a x=0 y=0 z=0
Se 2c x=0 y=1/2 z=0.26

PNAS

Superconductivity in the PbO-type structure α-FeSe

Fong-Chi Hsu*†, Jiu-Yong Luo*, Kuo-Wei Yeh*, Ta-Kun Chen*, Tzu-Wen Huang*, Phillip M. Wu‡, Yong-Chi Lee*, Yi-Lin Huang*, Yan-Yi Chu*†, Der-Chung Yan*, and Maw-Kuen Wu*§

*Institute of Physics, Academia Sinica, Nankang, Taipei 115, Taiwan; †Department of Materials Science and Engineering, National Tsing Hua University, Hsinchu 30013, Taiwan; and ‡Department of Physics, Duke University, Durham, NC 27708

Contributed by Maw-Kuen Wu, July 28, 2008 (sent for review July 28, 2008)

The recent discovery of superconductivity with relatively high transition temperature (Tc) in the layered iron-based quaternary oxypnictides La[O1−xFx] FeAs by Kamihara *et al.* [Kamihara Y, Watanabe T, Hirano M, Hosono H (2008) Iron-based layered superconductor La[O1-xFx] FeAs (x = 0.05–0.12) with Tc = 26 K. *J Am*

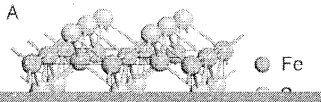

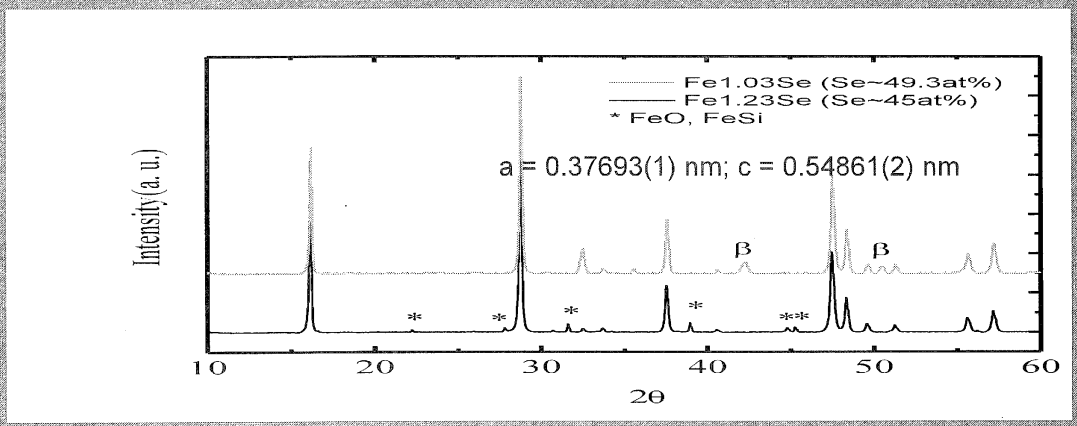

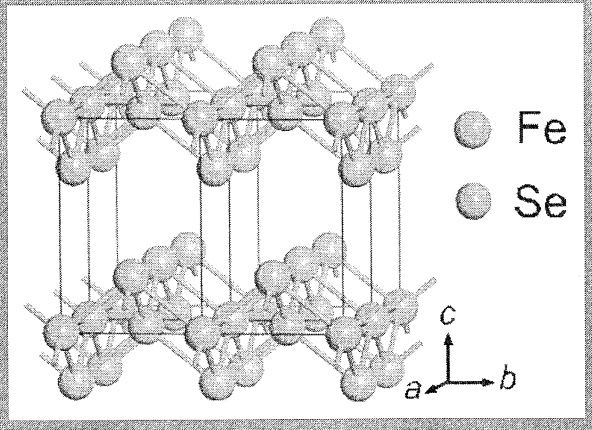

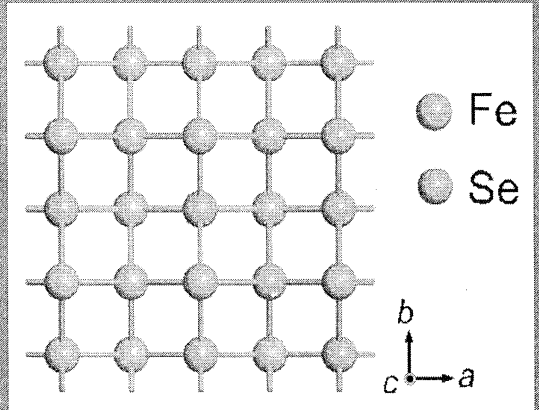

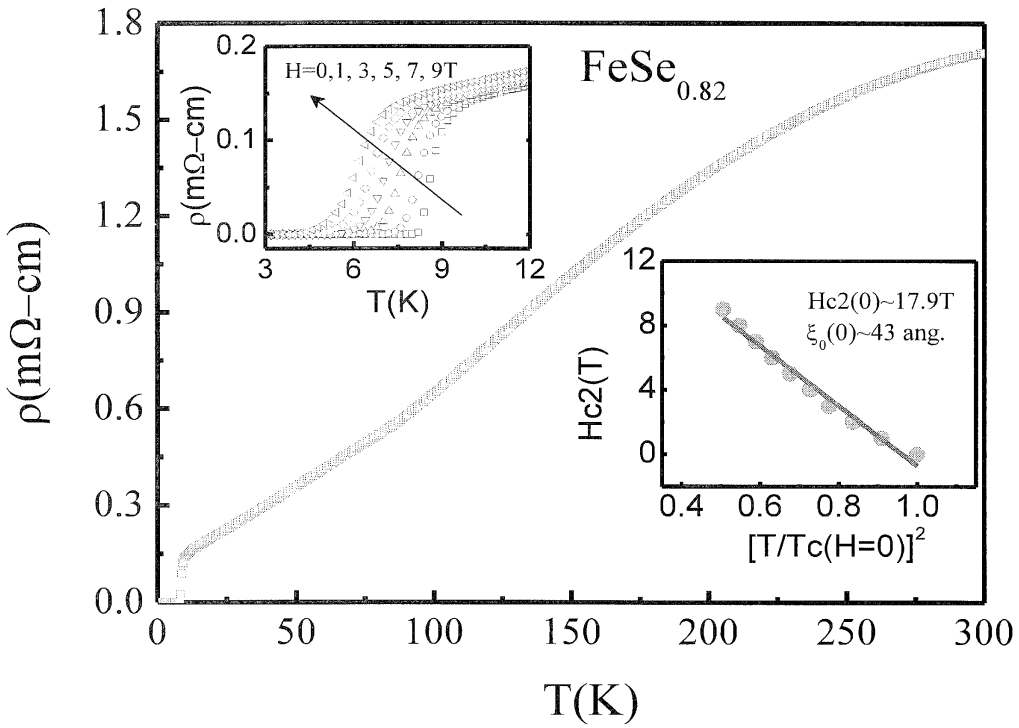

Preparation of Bulk $FeSe_{1-x}$

Processes worked out by T.M. McQueen *et. al.* (arXiv:0811.1613v1 2008)

1.Samples were prepared from freshly polished iron pieces and selenium shot;

2.Samples are sealed under vacuum in silica tubes with a piece of carbon;

3.Temperature was raised and held at 750 °C and then increased to 1075 °C for extra three days, followed by a fast decrease to 420 °C and held for two days before quenched in -13 °C brine.

4.The samples were annealed at various temperatures (300 ~ 500 °C) for two days followed by quenching in -13°C brine.

Single Crystal Growth (Flux Method)

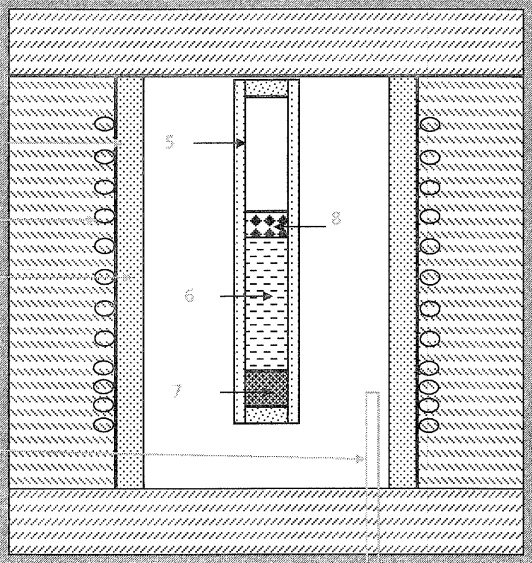

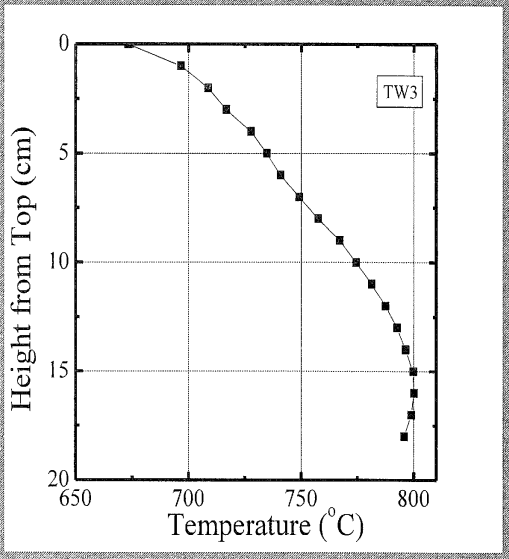

1. Stoichiometriy weights of Fe and Se powders were mixed with KCl to give a $FeSe_x$ (x=0-0.15) to KCl ratio of 1.5:10.
2. These powders were filled into quartz crucibles and the cr d sealed
3. The cr held there l ution.
4. Then .2 °C. During collect in size with ti
5. Later the crucible was cooled to room temperature while annealing at 400 °C for 20-25 hours before cooling to room temperature.

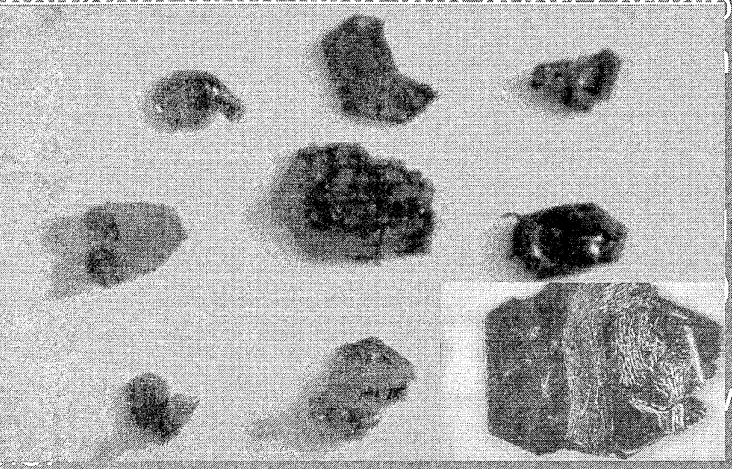

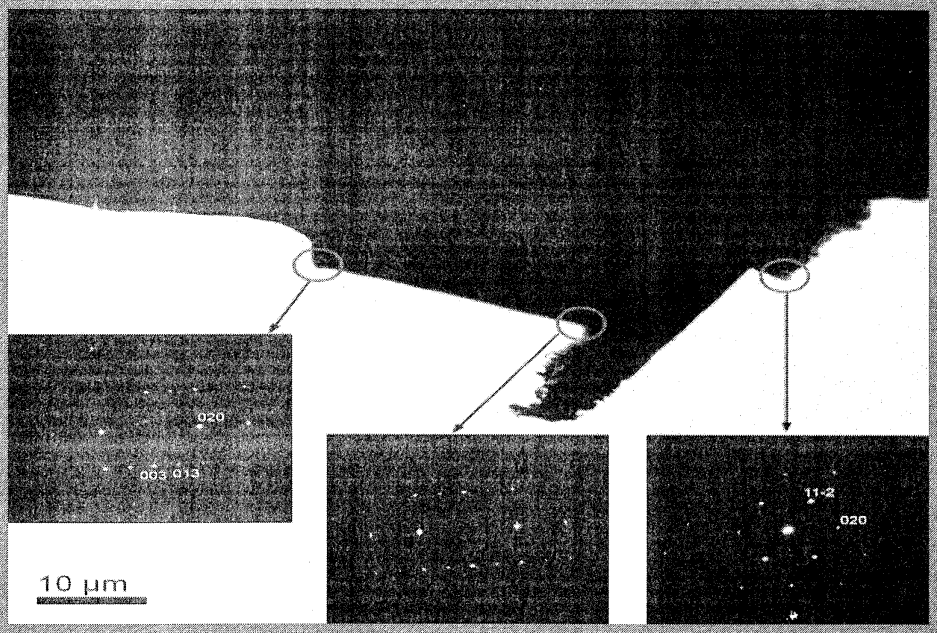

Low magnification view of $FeSe_{0.88}$ crystal in TEM. Three electron diffraction patterns are shown with their corresponded area of interests. Note that the patterns were taken at a different magnification where the image would suffer a certain degree of rotation. Weak spots in the right zone-axis pattern are from double diffraction. Only tetragonal-FeSe phase was observed in the above three thin areas.

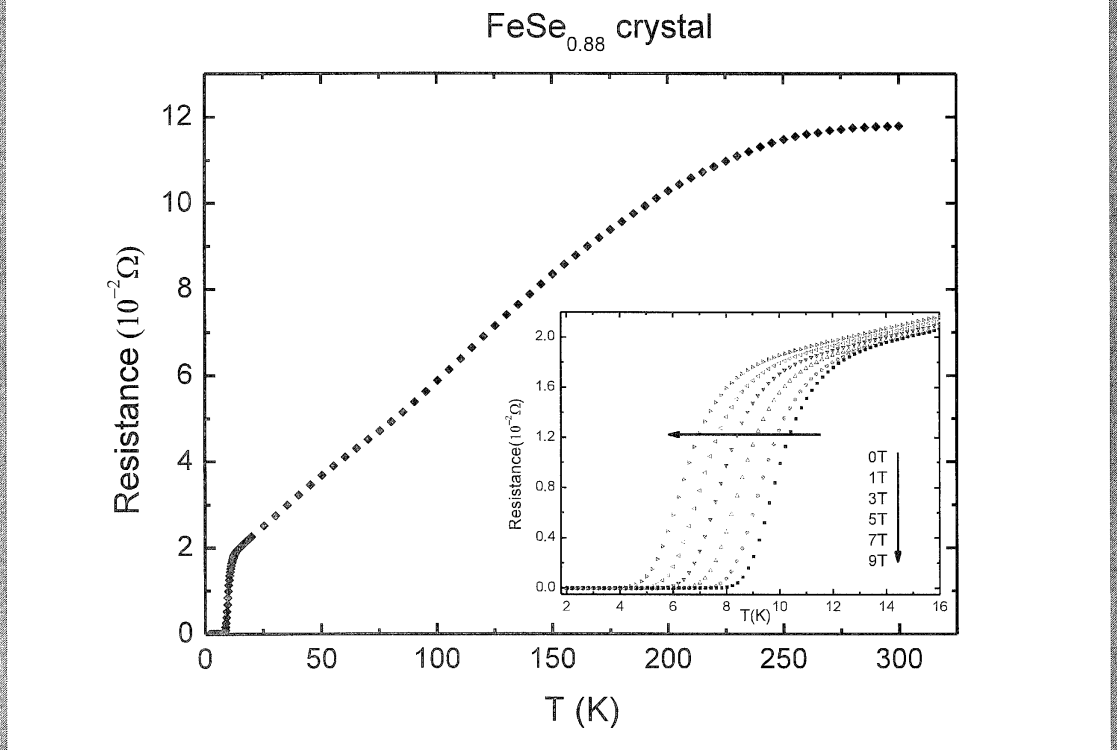

OUTLINE

- Single Crystal Growth of α – FeSe
- Fabrication of α – FeSe(Te) Thin Films
- Some properties of FeSe Superconductor
  - Transport properties
  - Magnetic properties
  - Specific heat
  - Structural Instability and Superconductivity
- Summary

Thin Film by PLD

1. Use targets of roughly 1”×8mm
2. Thin films were deposited in a vacuum chamber (~10^{-5} Torr) using a KrF (λ = 248 nm) excimer laser
3. The power density of focused laser on the target is 5~6 J/cm^2, and the repetition rate is 2 Hz.
4. The target-substrate distance is near 50 mm.
5. The substrate temperature of deposition is varied from 250 °C to 500 °C.
6. The deposition rate of thin film is about 0.5Å/shot. In addition,
7. the surfaces of targets were polished before each deposition to improve the reproducibility.

FeSe(Te) Thin Films

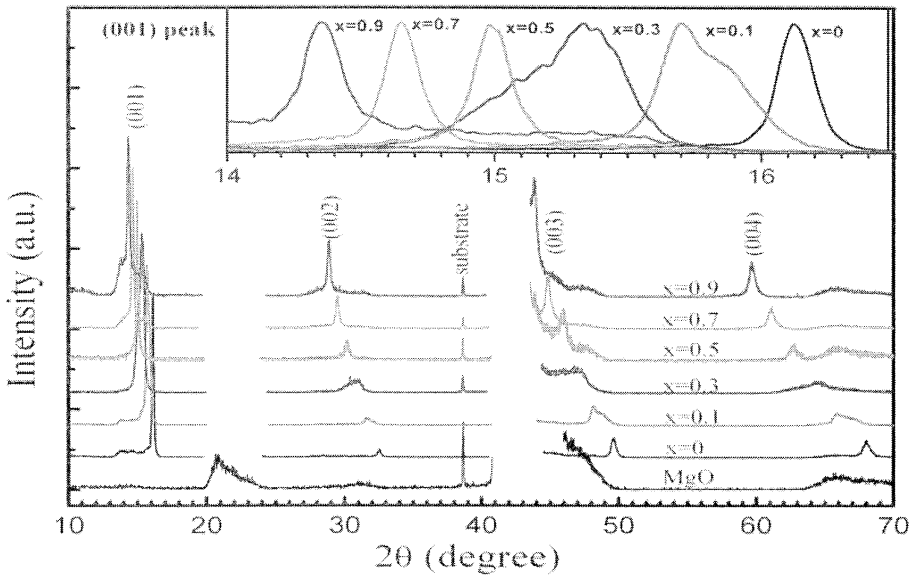

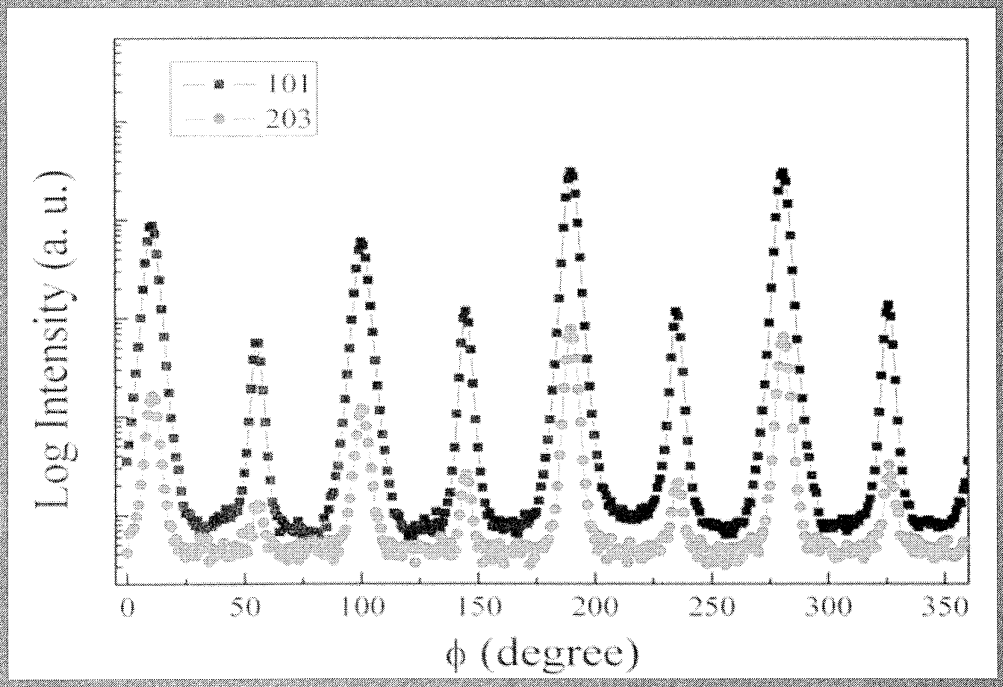

The Φ-scan of (101) and (203) peaks of FeSe(Te) films. Two domains with 4-fold symmetry are observed, which is 45° rotated to each other. The orientation of major domain is 45° rotated related to the a-axis of substrate.

FeSe(Te) Thin Films

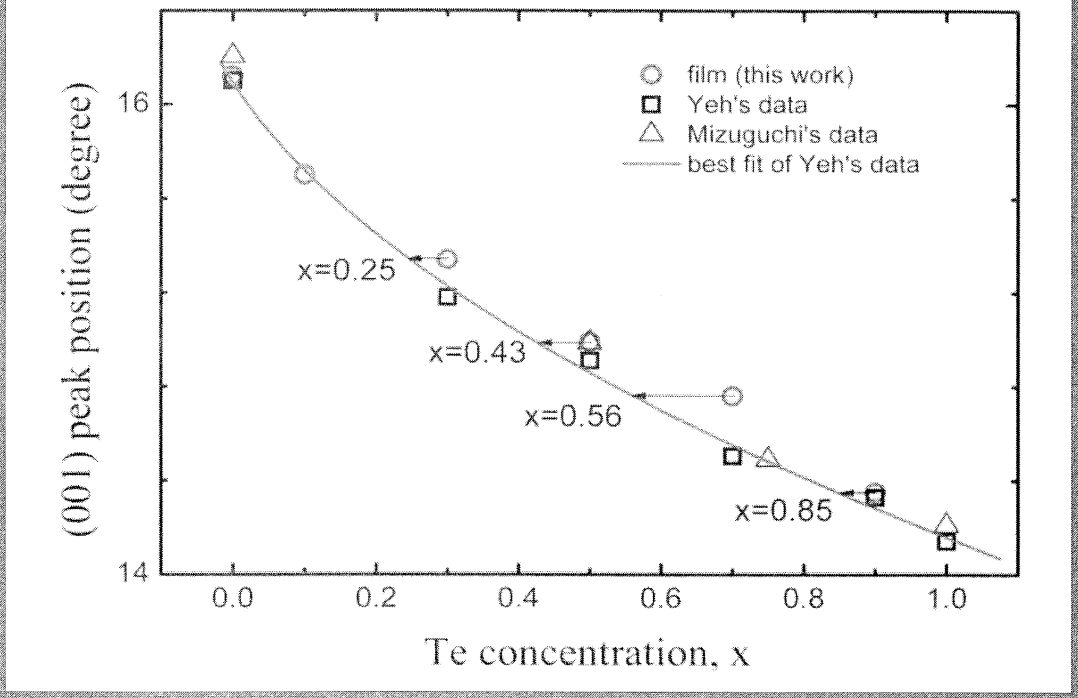

FeSe(Te) Thin Films

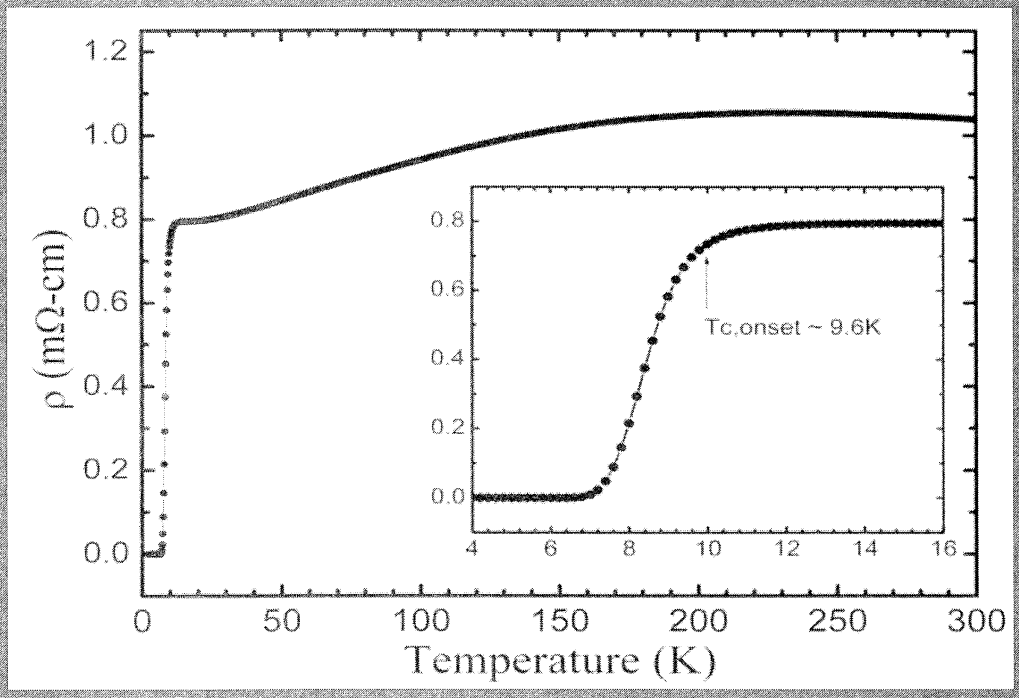

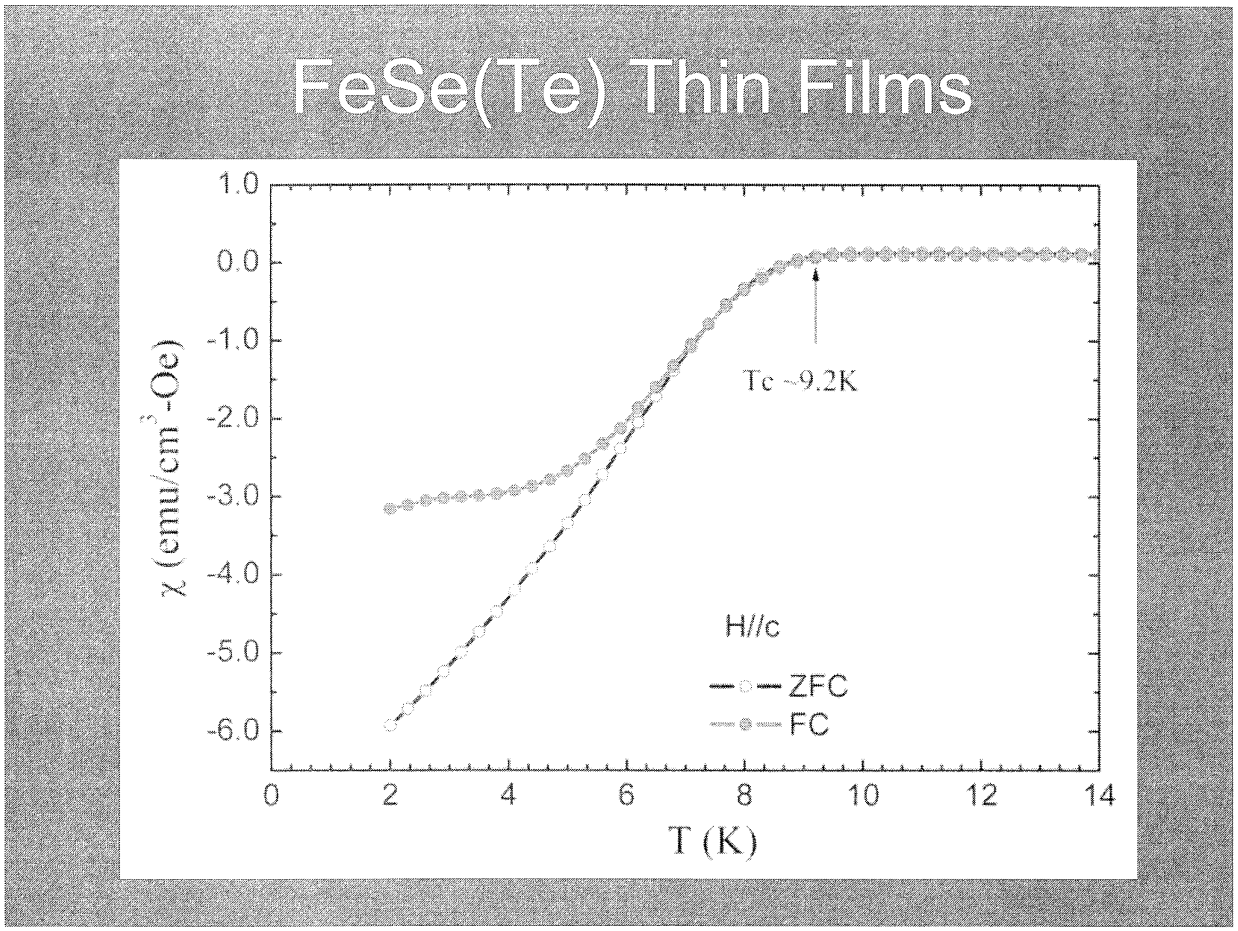
FeSe(Te) Thin Films
χ (emu/cm³-Oe)
T (K)
Tc ~9.2K
H//c
ZFC
FC

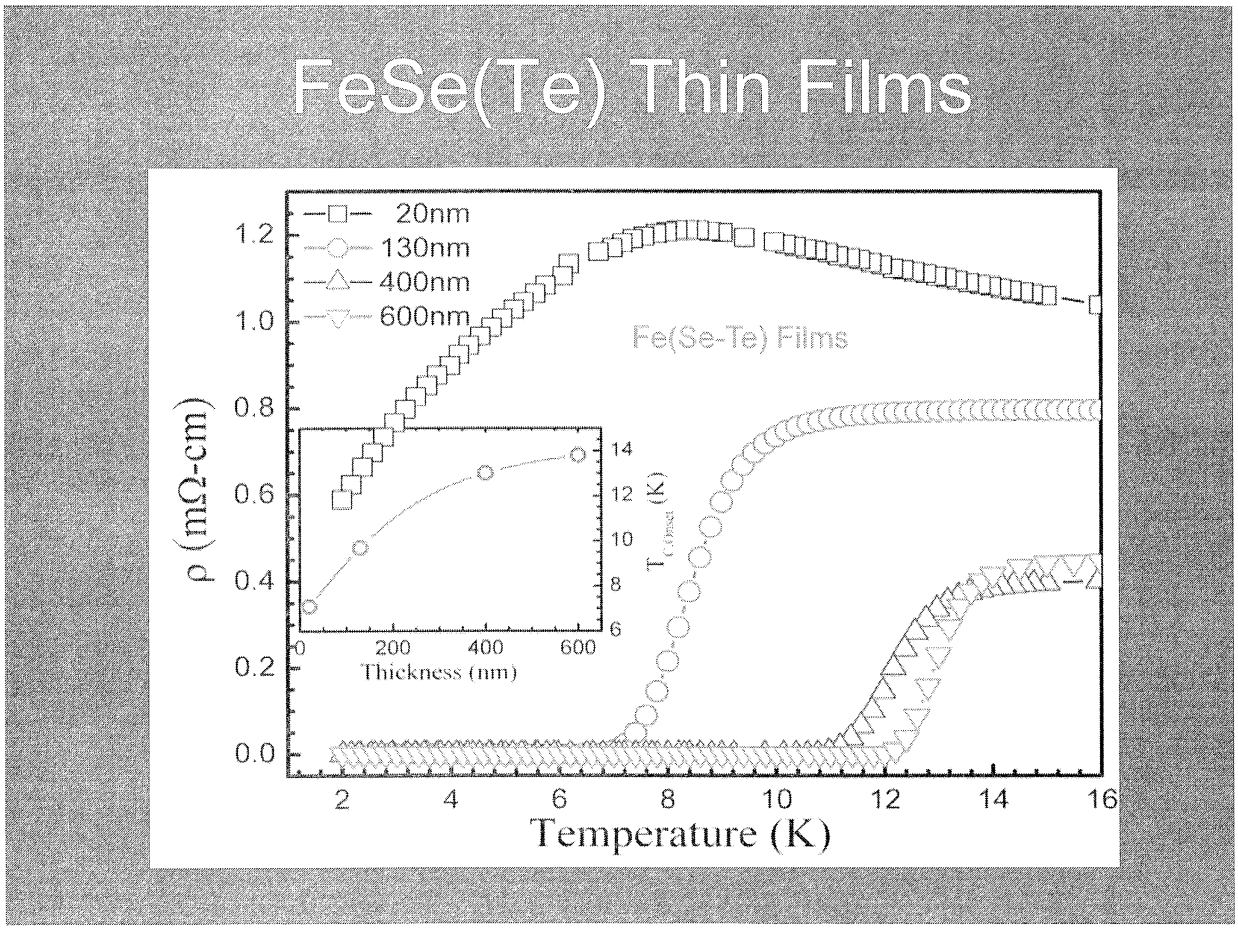
FeSe(Te) Thin Films
20nm
130nm
400nm
600nm
Fe(Se-Te) Films
ρ (mΩ-cm)
Temperature (K)
Thickness (nm)

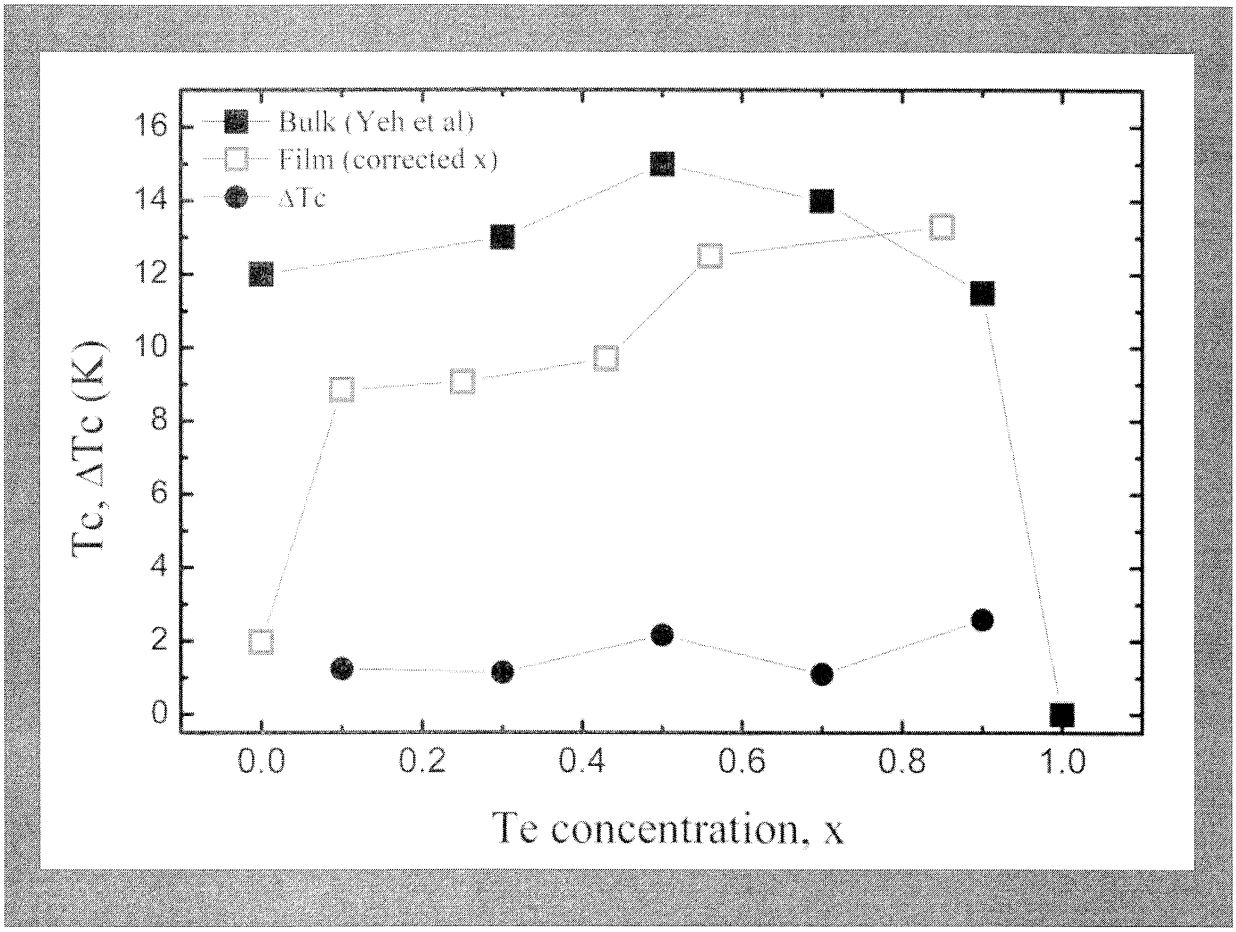

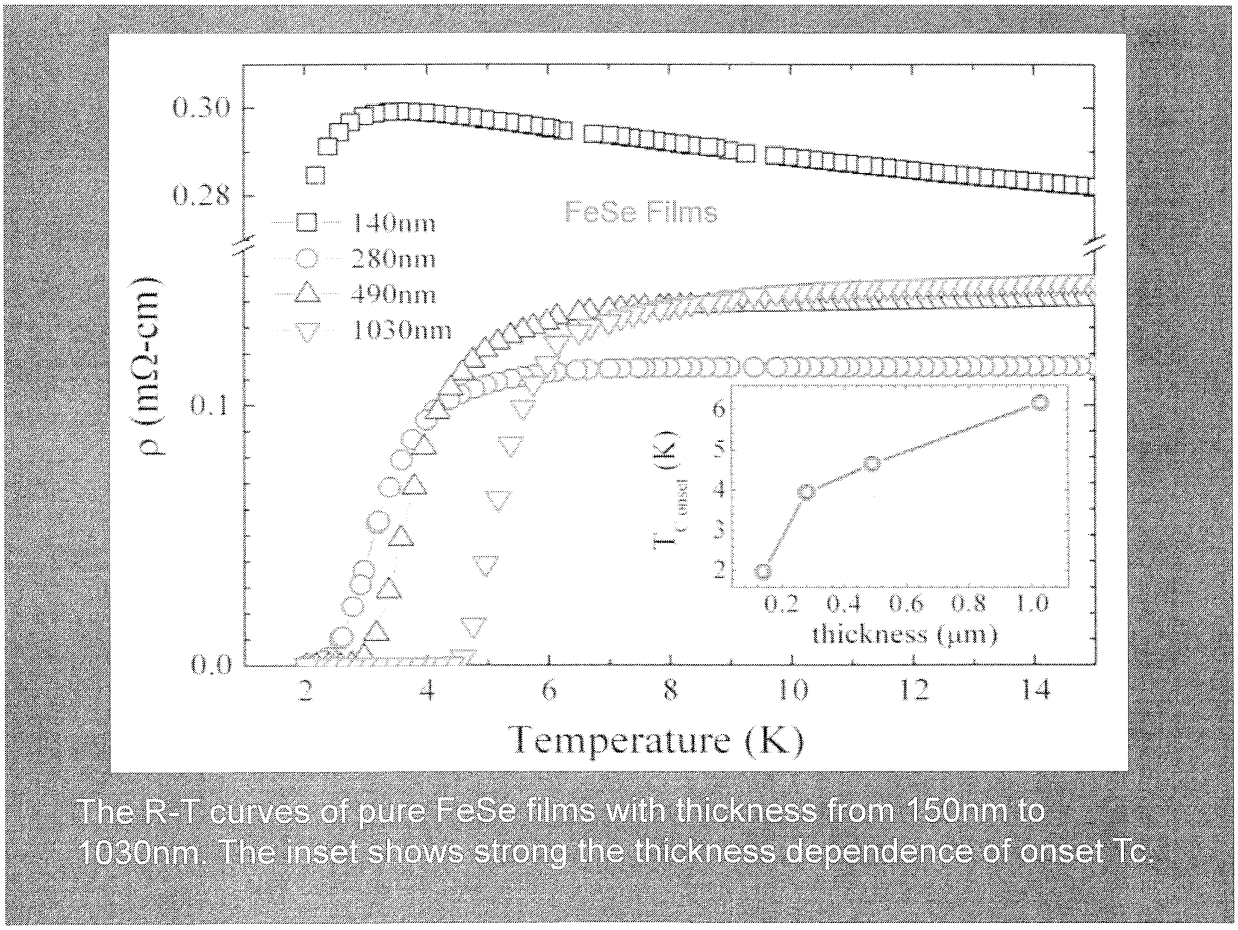

The R-T curves of pure FeSe films with thickness from 150nm to 1030nm. The inset shows strong the thickness dependence of onset Tc.

OUTLINE

- Single Crystal Growth of α – FeSe
- Fabrication of α – FeSe(Te) Thin Films
- Some properties of FeSe Superconductor
  - Transport properties
  - Magnetic properties
  - Specific heat
  - Structural Instability and Superconductivity
- Summary

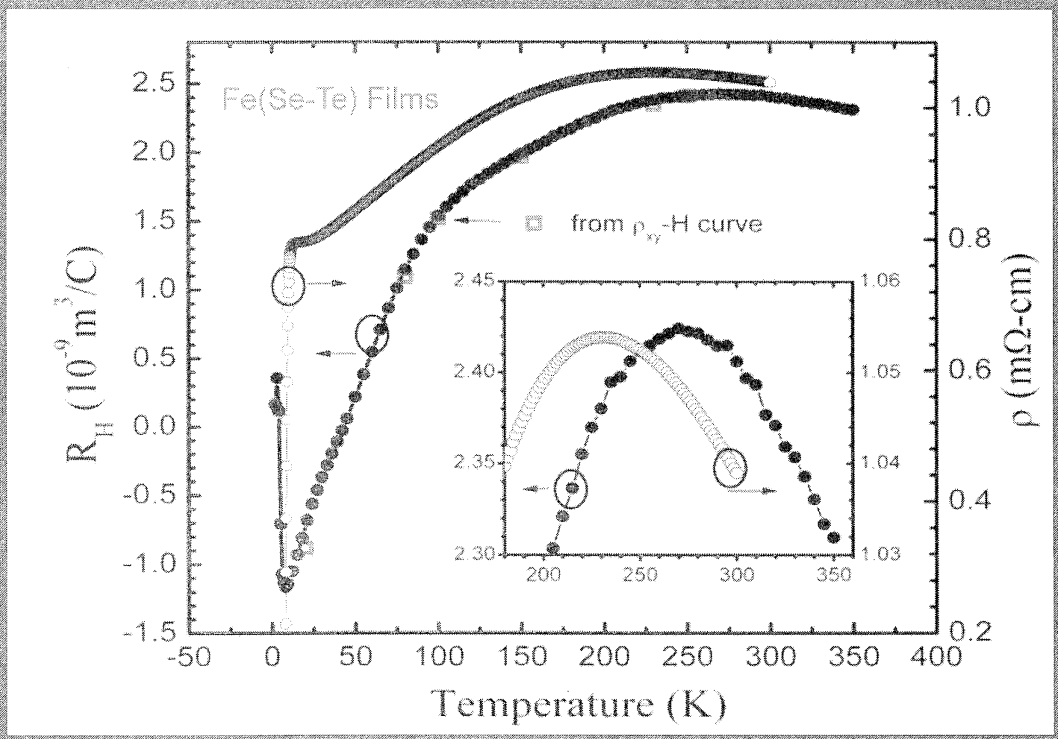

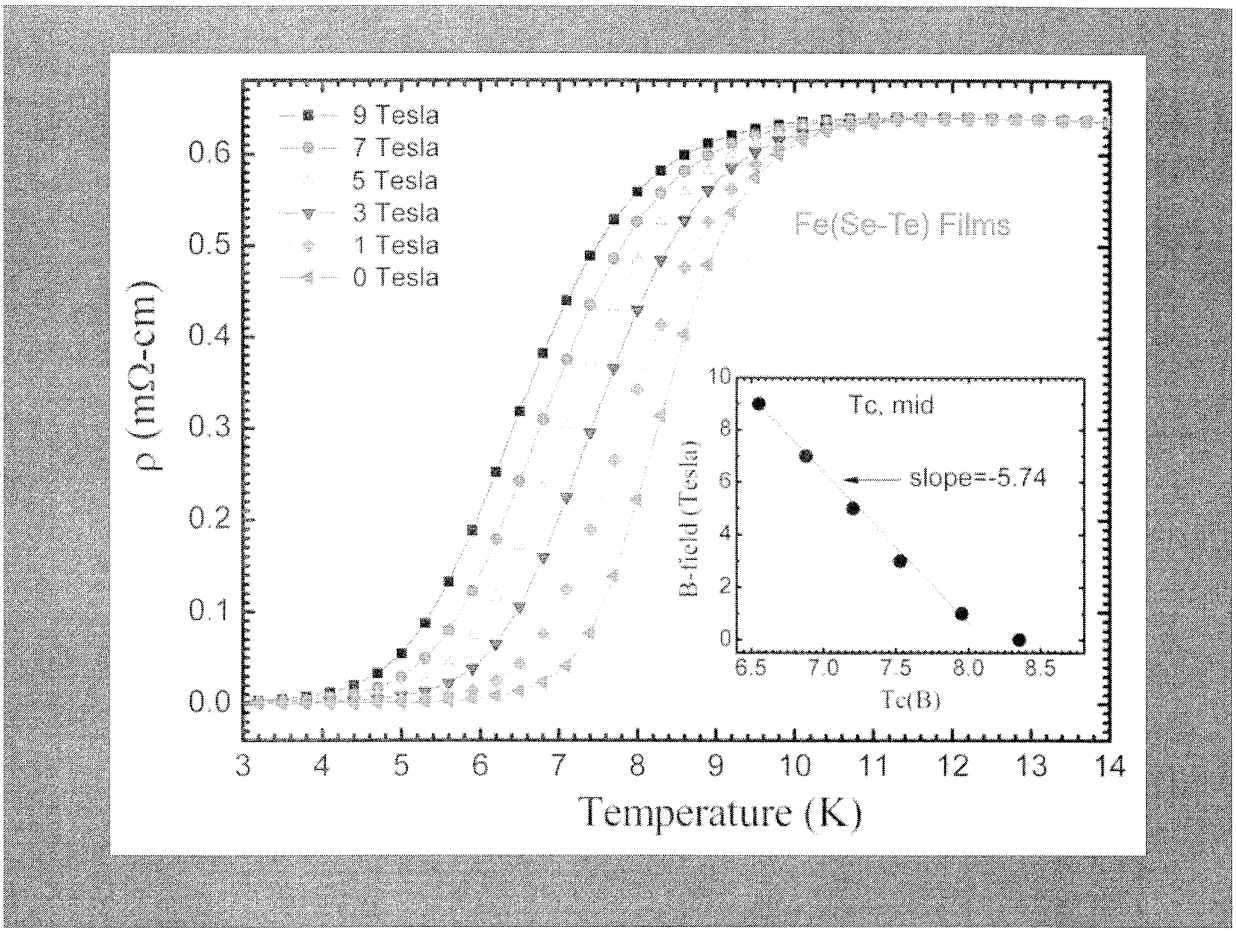
9 Tesla
7 Tesla
5 Tesla
3 Tesla
1 Tesla
0 Tesla
Fe(Se-Te) Films
ρ (mΩ-cm)
Temperature (K)
Tc, mid
slope=-5.74
B-field (Tesla)
Tc(B)

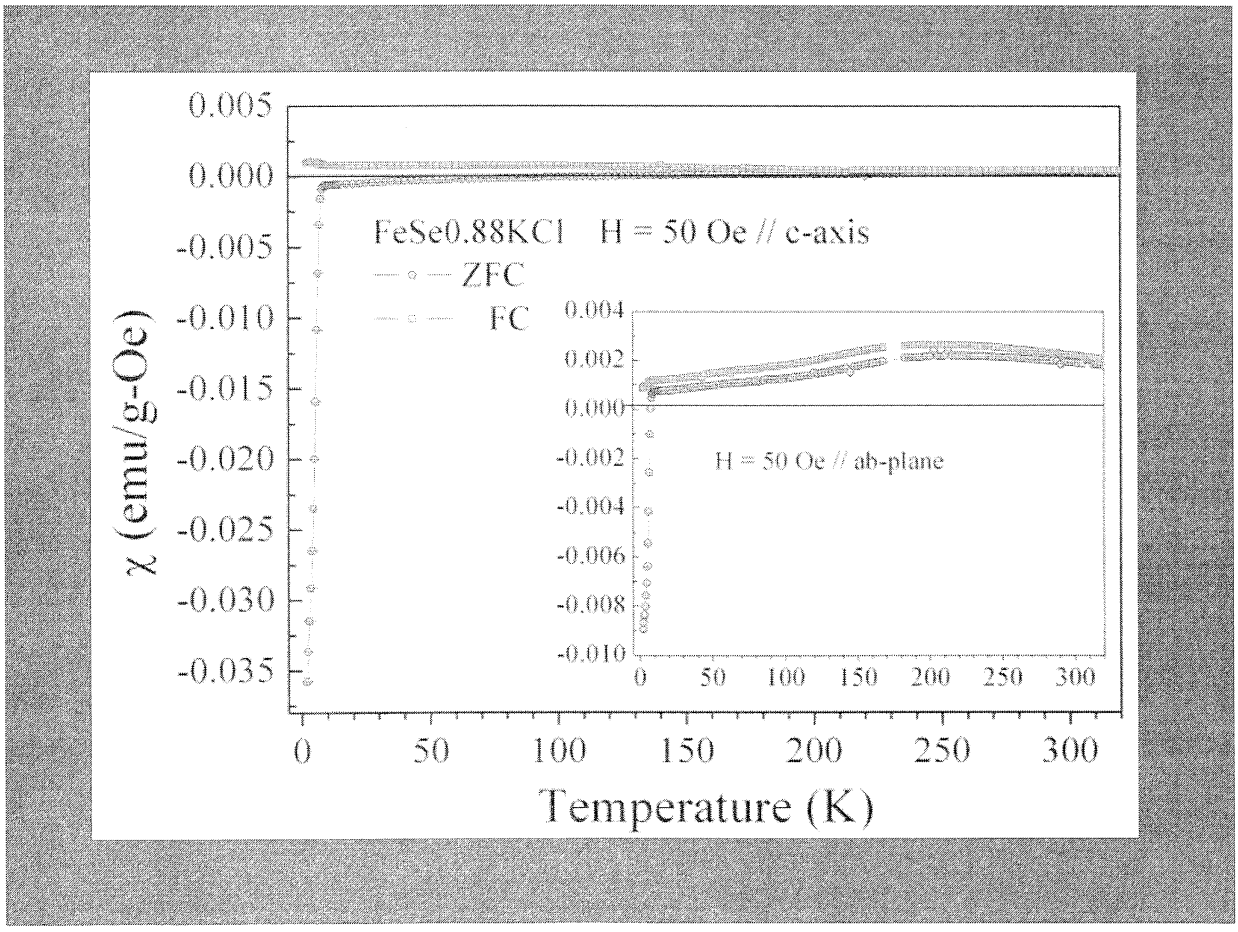
FeSe0.88KCl H = 50 Oe // c-axis
ZFC
FC
H = 50 Oe // ab-plane
χ (emu/g-Oe)
Temperature (K)

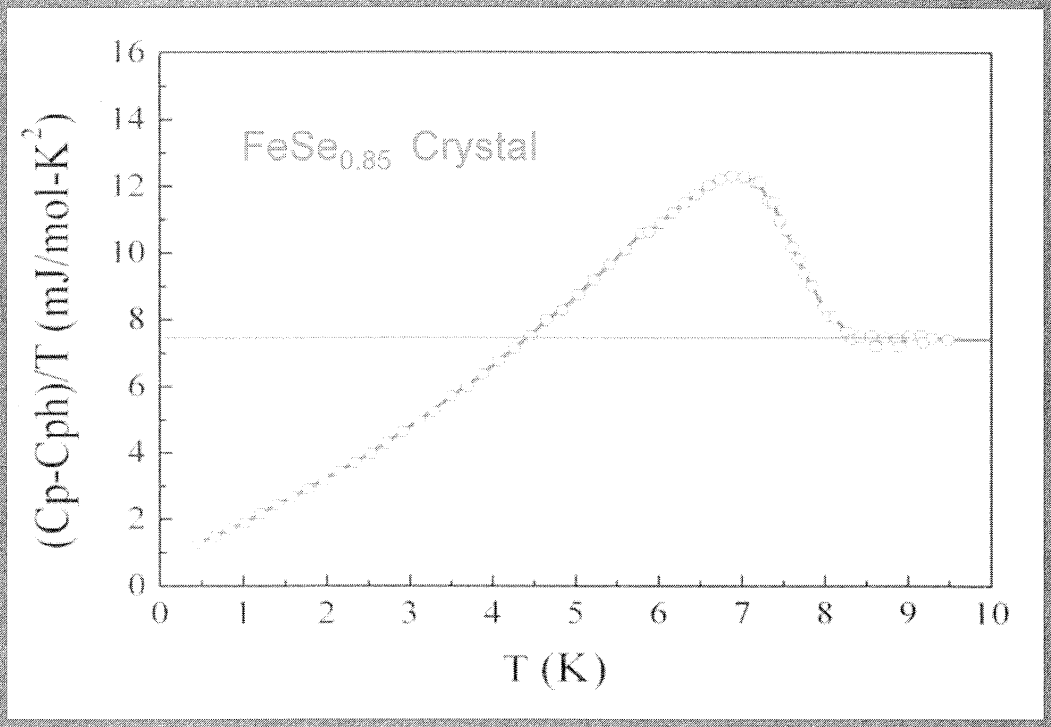

Temperature dependence of (Cp-Cph)/T in a magnetic field of 0 G. The phonon contribution Cph is $0.586T^3$-$1.39E\text{-}4T^5$. A dotted line represents constant electronic specific heat 7.45 mJ/mol-K^2 for comparison.

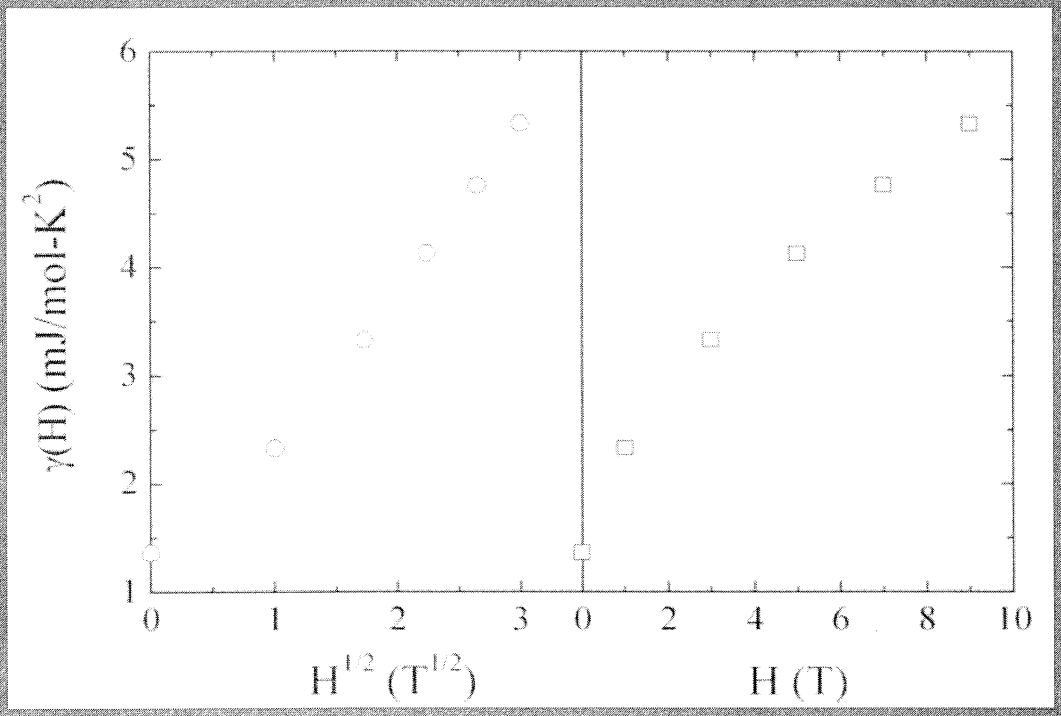

The magnetic field dependence of electronic specific heat of the $FeSe_{0.88}$ sample. The left figure shows the plot of $\gamma(H)$-$H^{1/2}$ and the right one shows the plot of $\gamma(H)$-H.

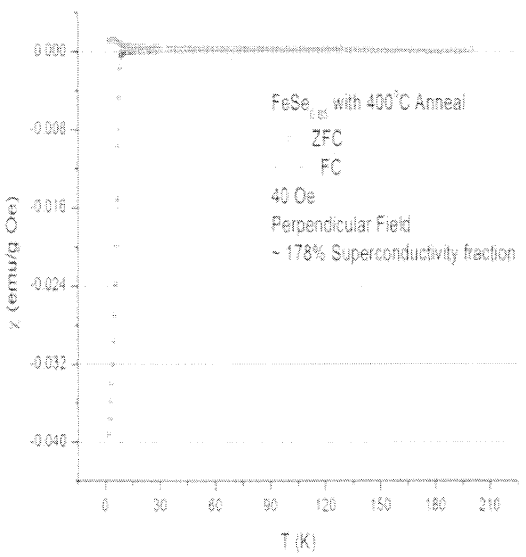

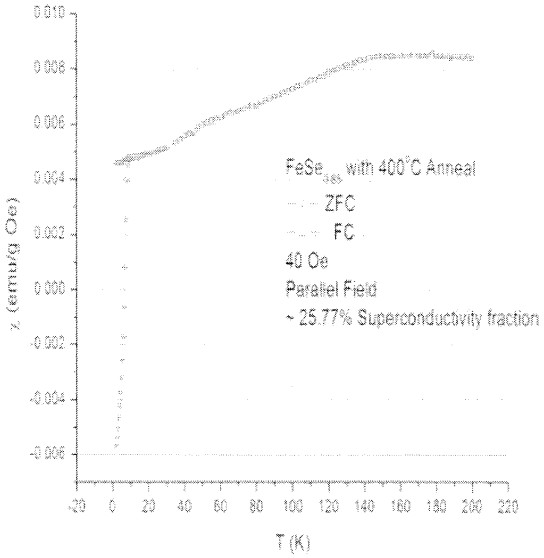

Wilson ratio $$R_W = \frac{\pi^2 k_B^2}{3\mu_B^2}\left(\frac{\chi_{ab}(0)}{\gamma}\right) >> 1$$

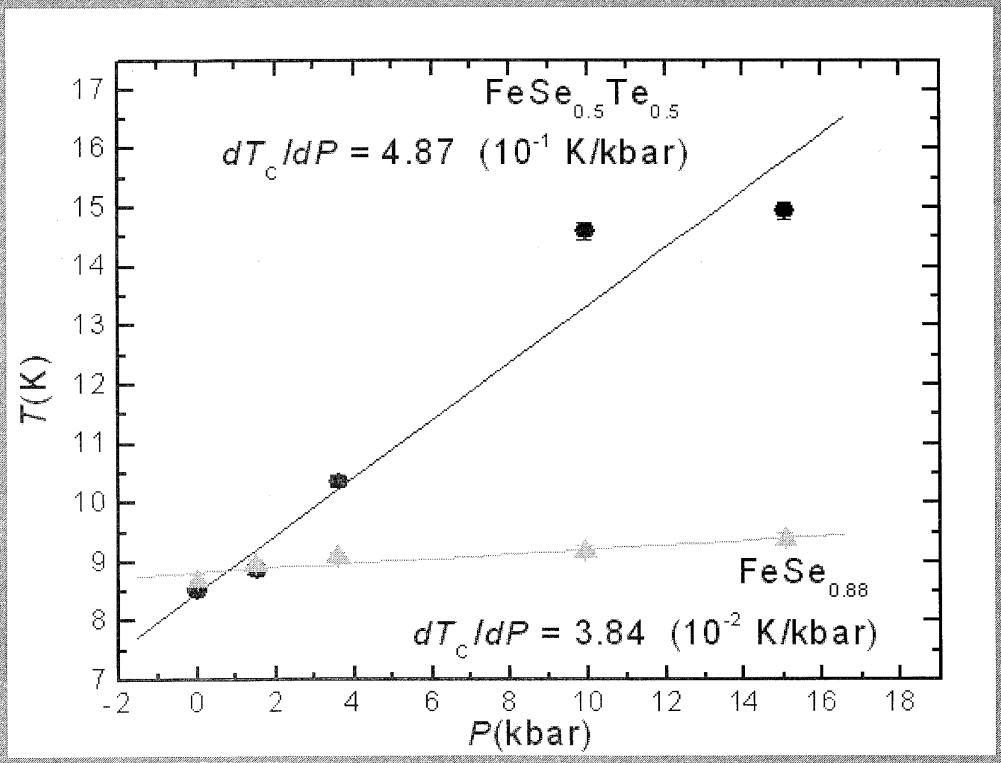

$FeSe_{0.82}$

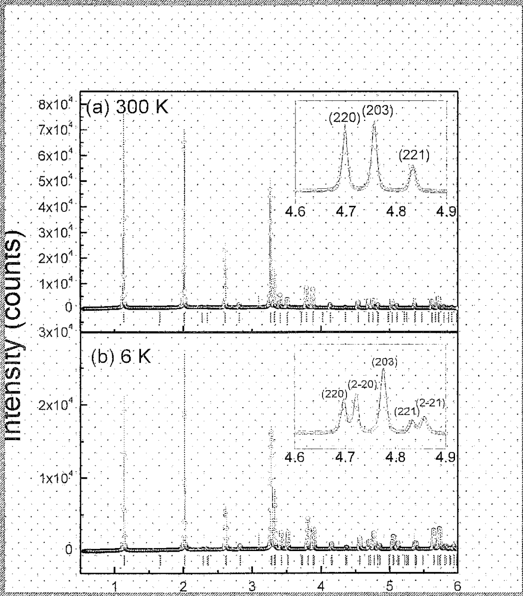

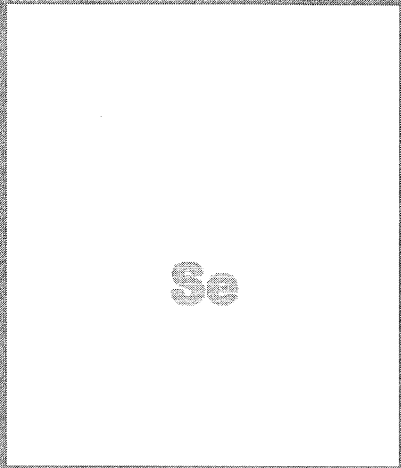

	a (Å)	b (Å)	c (Å)	α	β	γ
300K	[illegible]	[illegible]	[illegible]	90	90	90
6K	[illegible]	[illegible]	[illegible]	90	90	[illegible]

Temperature dependence of the X-ray powder diffractions for FeSe by synchrotron source at BL12b2 in SPring 8 with incident beam wavelength of 0.995 Å. Observed (open black circle) and calculated (red solid line) powder diffraction intensities of FeSe at (a) 300K using space group P4/nmm and (b) 6K using space group P-1. [illegible] Blue vertical lines show the Bragg peak positions.

structure parameter (Fe-Se)

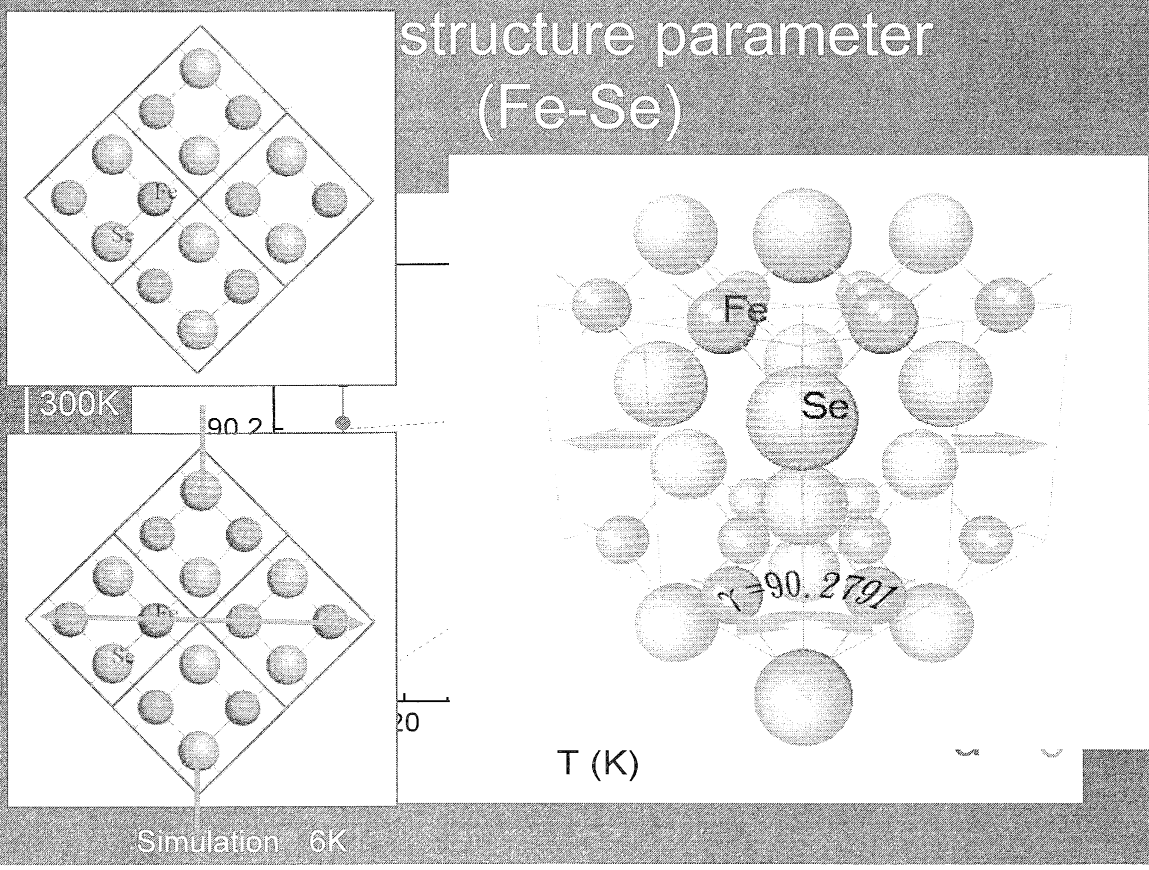

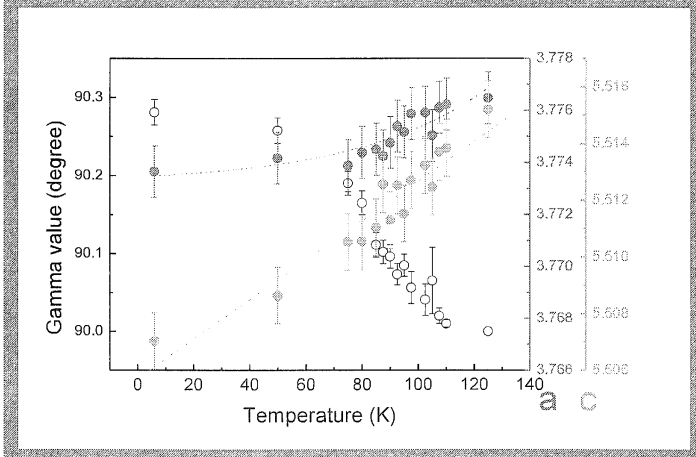

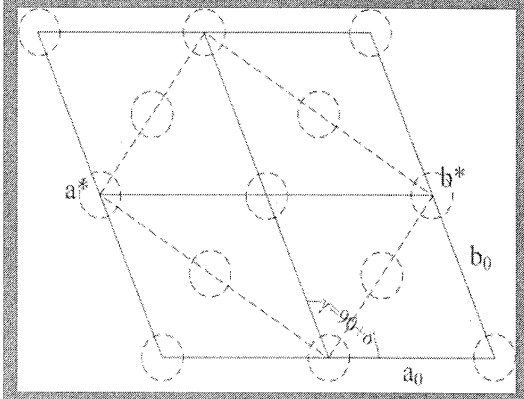

The temperature dependence of gamma value (open black circle), a (blue solid circle) and c (red solid circle) obtained from detailed X-ray refinement by P-1 space group.

The c is shirking as temperature decreasing with a gradient equals to $6.97X10^{-5}$ A/K. Oppositely, the shirking of a axis is obviously retarding as the phase transition occurring at 105 K.

FeTe

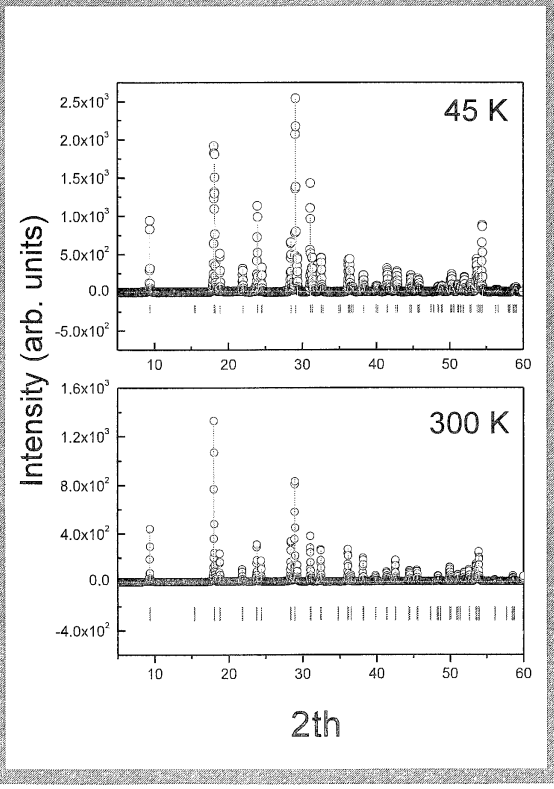

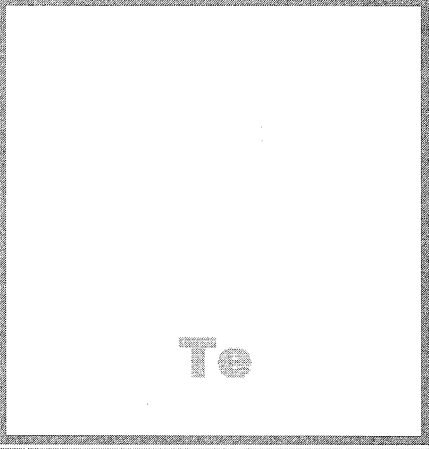

	a (Å)	b (Å)	c (Å)	γ
45K	3.824	3.854	6.303	90
300K	3.861	3.861	6.319	90

Temperature dependence of X-ray diffraction for FeTe using λ=1.0333 Å

The fitting results shows the different shrinking behavior between FeTe and FeSe. The FeTe compounds become a triclinic crystal which a≠b ≠ c and γ =90. This results might cause from the occupancy of Te is 80% and the larger atom size.

$FeSe_{0.5}Te_{0.5}$

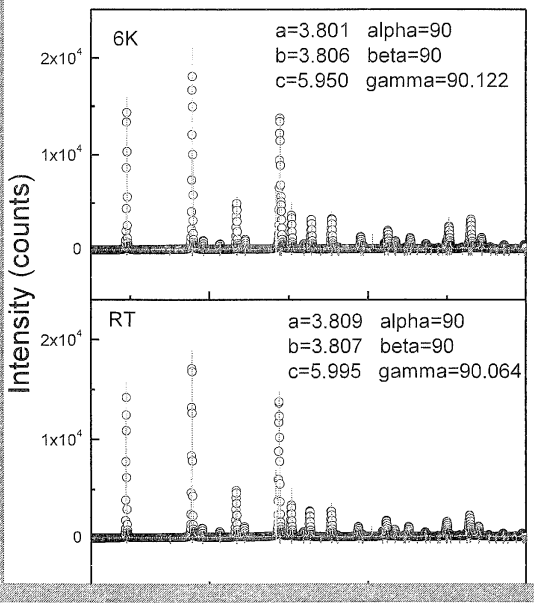

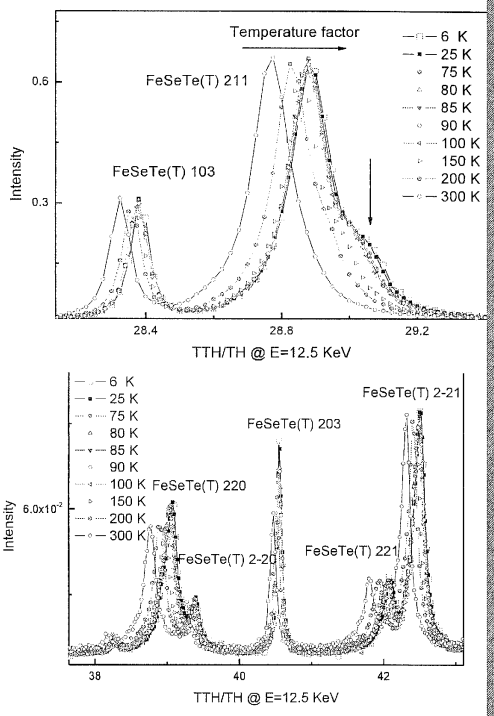

The sketchs for distortion of $FeSe$,$FeSe_xTe_{1-x}$, $FeSe_xS_{1-x}$ and FeTe

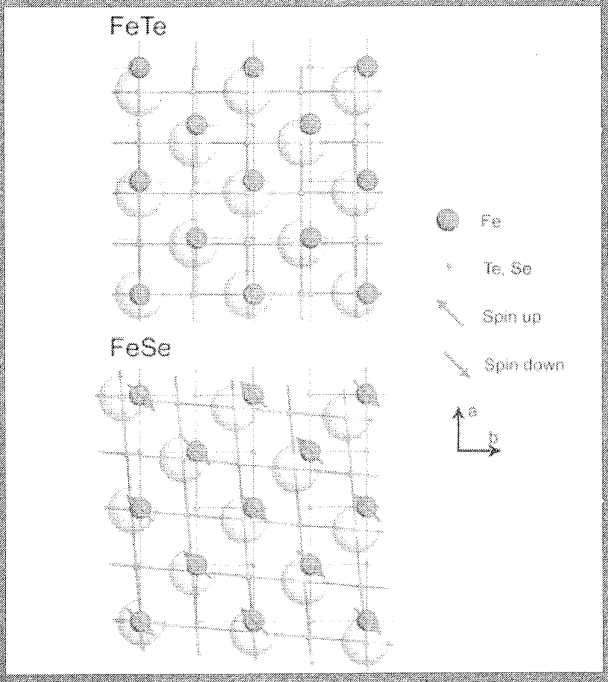

First neighbors J_1 ,frustrated

Strong J_2 : AF

Caused by the shrinking ratios are different on a, b axis, the symmetry along the (110) axis destroy after distortion occurred. This means the anti-ferromagnetic ordering might be break in and coherence length of spin fluctuation would be shorter than one of FeSe.

The symmetry along the (110) axis does not destroy and fluctuation of spin at low temperature might still exist.

$Fe_{1-x}SeTm_x$

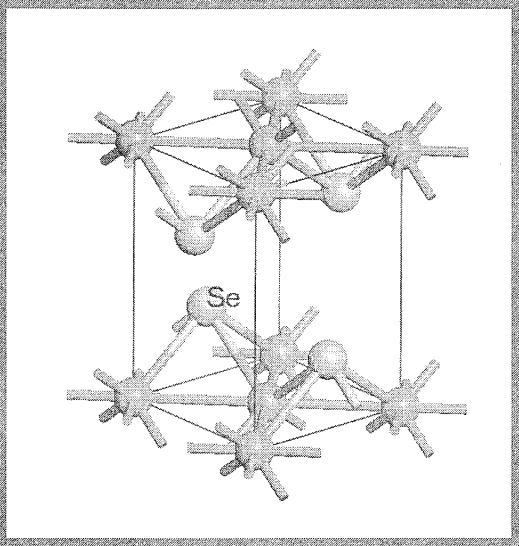

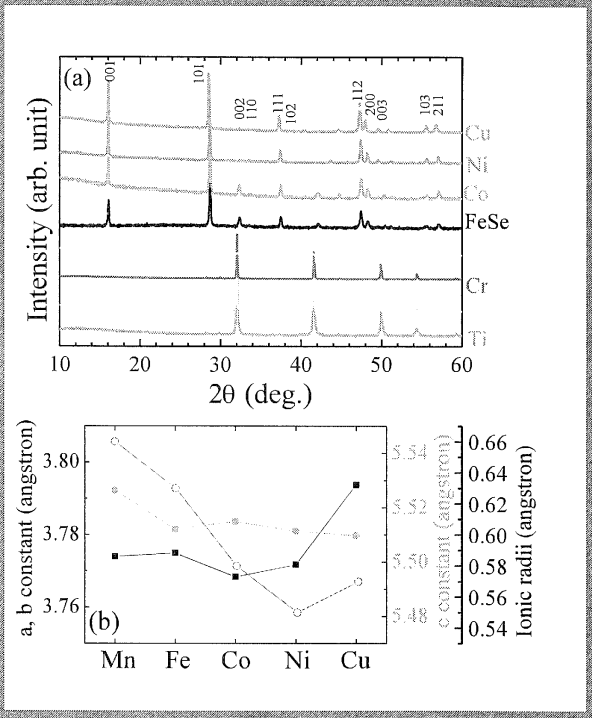

21	22	23	24	25	26	27	28	29	30
Sc	Ti	V	Cr	Mn	Fe	Co	Ni	Cu	Zn
Scandium	Titanium	Vanadium	Chromium	Manganese	Iron	Cobalt	Nickel	Copper	Zinc
44.955910	47.867	50.9415	51.9961	54.938049	55.8457	58.933200	58.6934	63.546	65.409

$Fe_{1-x}SeCu_x$

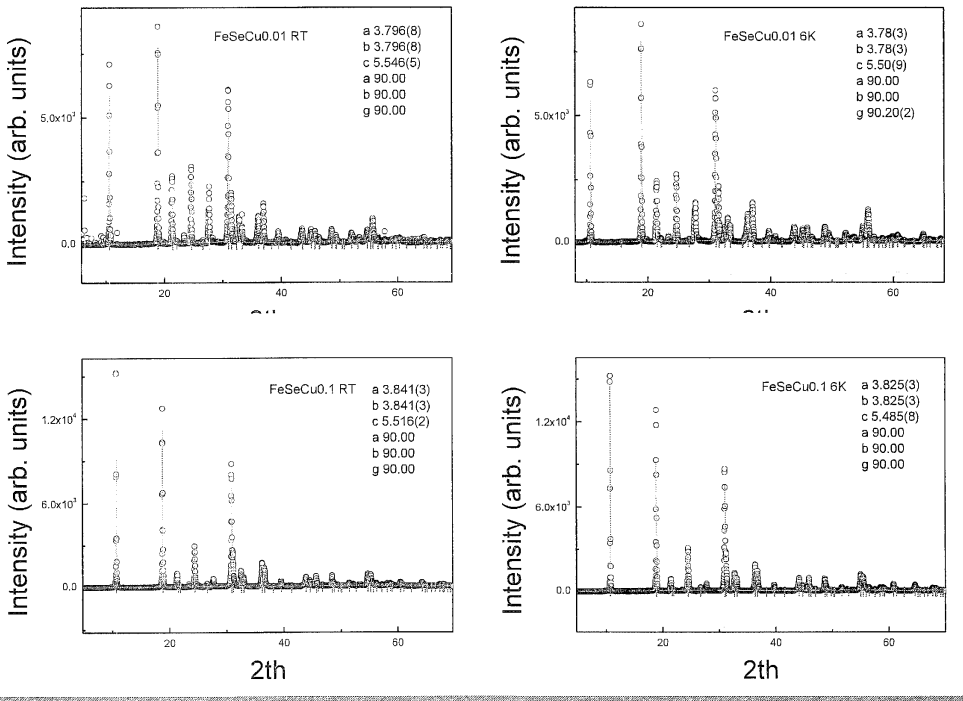

$Fe_{1-x}SeCu_x$

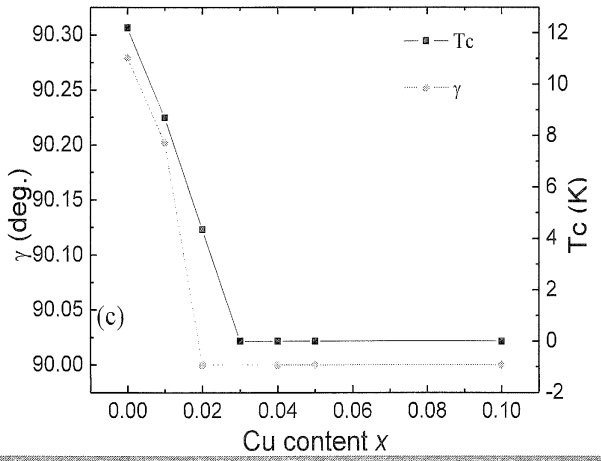

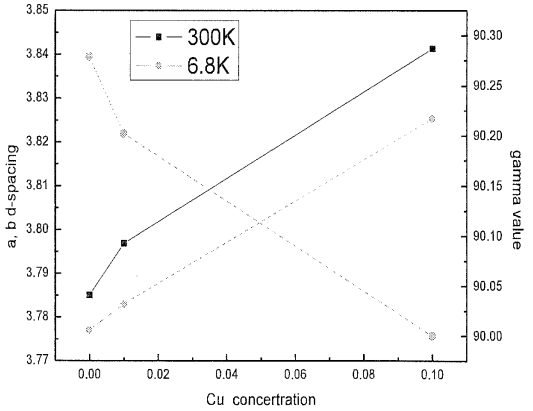

$(Fe_{0.9}Mn_{0.1})Se_{0.85}$

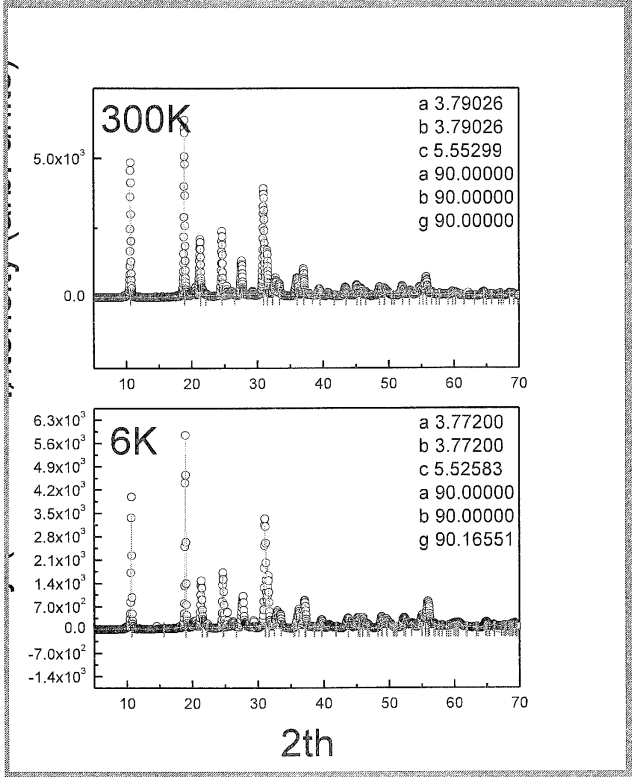

FeSe+Mn0.1

	a (Å)	b (Å)	c (Å)	γ
6K	3.772	3.772	5.526	90.166
300K	3.790	3.790	5.552	90

Neutron diffraction for $Fe_{0.9}Mn_{0.1}Se$

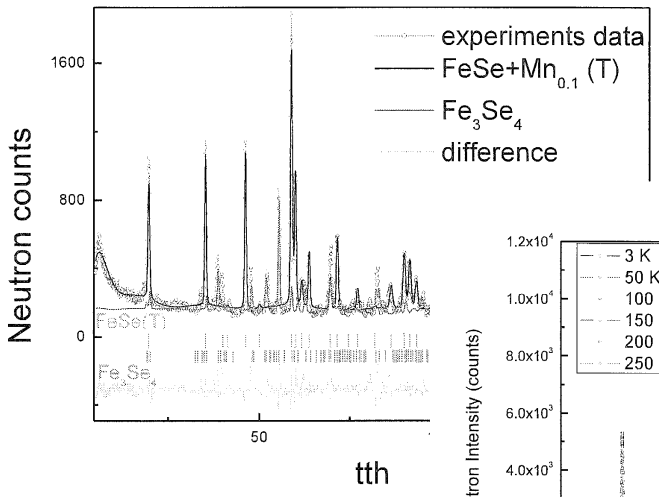

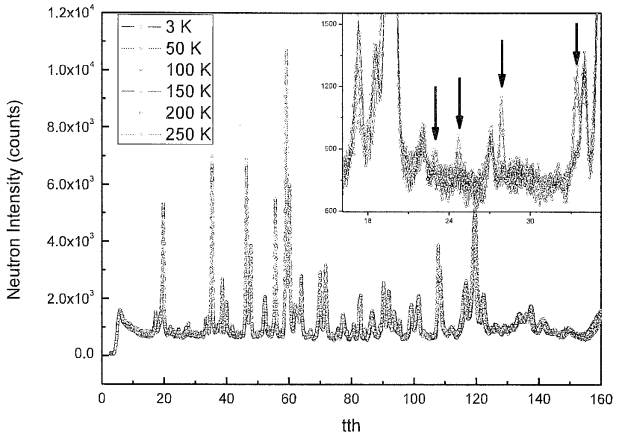

Neutron diffraction for $Fe_{0.9}Cu_{0.1}Se$

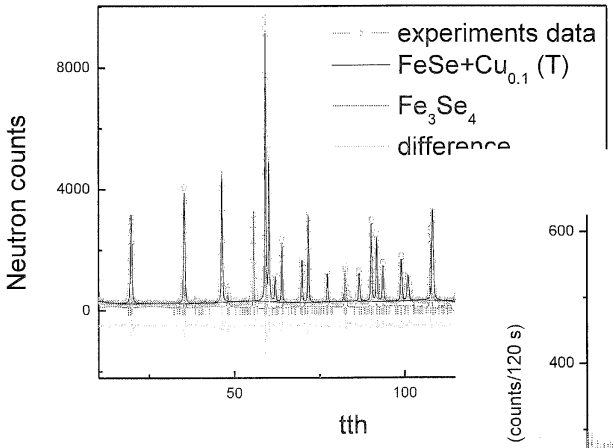

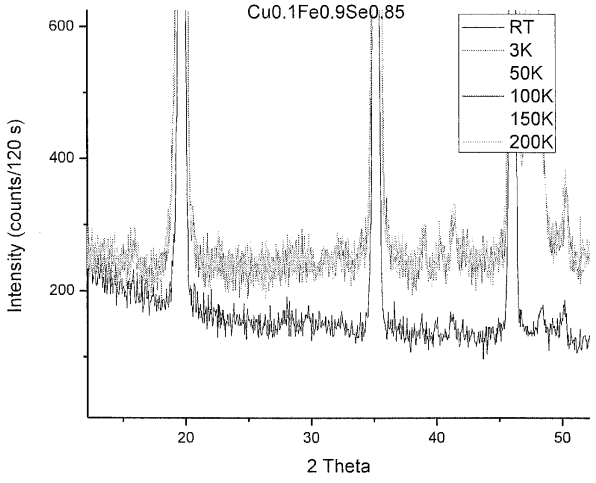

Table X. The critical temperature of superconducting, phase transition temperature and gamma angle for iron selenide

``	Tc	Phase transition temperature	**Gamma angle (°) at 6 K
$FeSe_{0.88}$	8.? K	~105K	90.279
FeTe	none	~80K *	90
$Fe(Se_{0.5}Te_{0.5})$	15.2 K	~100K	90.122
$(FeMn_{0.1})Se$	11.2 K	~85K	90.166
$(FeCu_{0.1})Se$	none	none	90

Summary

- Single crystal and oriented thin films can be prepared, but quality still need improvement
- Anisotropic magnetic susceptibility in normal state is observed
- A low temperature distortion from tetragonal phase (P4/mmm) to triclinic phase (P-1) phase is essential for superconductivity
  - FeSe –γ-angle increases from 90° to about 90.3° at ~ 105K; Tc correlates well with inverse of c-lattice parameter (1/c)
  - Te-doping has highest Tc with largest γ; Te-doping enhances H_{c2} and Tc due to more 2D charcteristics; pressures effect on Tc of Te-doped sample is much larger than that of Fe-Se
  - 3d-metal doping only Mn sustains superconductivity; the other dopants either suppress low-T structural distortion (Cu-doping) or do not form alpha-phase
- Unusual pressure induced reversible amorphization of FeSe(Te) is observed

Acknowledgments

1. Academia Sinica—F.C. Hsu, J.Y. Luo, K.W. Wei, T.W. Huang, Y.C. Lee, Y.L. Huang, C.T. Ke, H.H. Chang, C.T. Wu, M.J. Wang
2. P.M. Wu, A.M. Chang (Duke Univeristy)
3. A. K. Stemshorn and Y. K. Vohra (UAB)
4. Australia Neutron Facility (ANTSO) for neutron scattering work
5. Financial supports from Taiwan NSC & US-AFOSR/AOARD

Thank You Very Much for Your Attention